Computational Exploration of Polymer Mechanochemistry: Quantitation of Activation Force and Systematic Discovery of Reaction Sites Utilizing Two Forces

Julong Jiang,*,[1] Koji Kubota,[2,3] Mingoo Jin,[2] Zhi Jian Wang,[2] Tasuku Nakajima,[2,4] Hajime Ito,[2,3] Jian Ping Gong,[2,4] Satoshi Maeda*,[1,2]

Affiliations

[1] Department of Chemistry, Faculty of Science, Hokkaido University, Sapporo, 060-8628, Japan.

[2] Institute for Chemical Reaction Design and Discovery (WPI-ICReDD), Hokkaido University, Sapporo 001-0021, Japan.
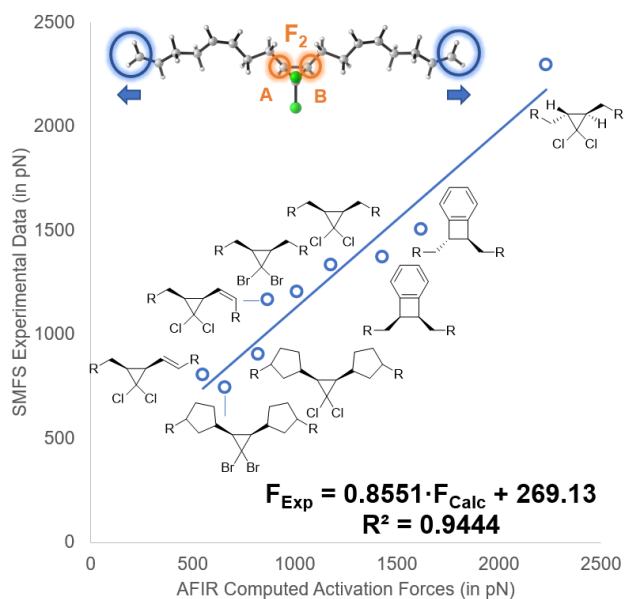
[3] Division of Applied Chemistry, Graduate School of Engineering, Hokkaido University, Sapporo, 060-8628, Japan

[4] Faculty of Advanced Life Science, Hokkaido University, Sapporo 001-0021, Japan

Corresponding authors:
jjiang.theochem@sci.hokudai.ac.jp
smaeda@eis.hokudai.ac.jp

$$F_{Exp} = 0.8551 \cdot F_{Calc} + 269.13$$
$$R^2 = 0.9444$$

Abstract

A series of mechanophores were studied computationally by employing the AFIR (Artificial Force Induced Reaction) method, which applies an artificial force on the molecule to trigger reactions, and meanwhile with a tensile force to simulate a mechanochemical reaction. The calculation results were both qualitatively and quantitatively consistent to those reported experimentally, indicating that the AFIR is a reliable approach to studying mechanochemical reactions. It was then applied to the study of retro-Diels-Alder reactions for the theoretical predictions of activation force levels which are currently unavailable. Moreover, it also helped to reveal the favored geometry for the enhancement of force effect. Later, the AFIR method was employed to study the mechanodegradation of generic polymers. The substituents effect and the polymer tacticity in strengthening the mechanical responsiveness, were highlighted by our study. Given the importance of cross-linker molecules in the double-network (DN) hydrogels, a fully automatic search of mechanochemical transformation pathways of a commonly used cross-linker molecule, *N,N'*-methylenebisacrylamide (MBAA), was also performed by the AFIR method. Through the work described in this article, we demonstrated that, in the field of polymer mechanochemistry, the AFIR method utilizing two forces is a simple but effective tool to give accurate predictions of activation force levels at any given timescale. In the meantime, the mechanistic study of mechanochemical reactions shown in this article is believed to provide insightful suggestions for the further design and application of mechanophores.

1. Introduction

Mechanochemistry, as one of the emerging fields in modern chemistry, is to use mechanical force to trigger chemical reactions. Sometimes, the mechanical force can prompt the reactions which cannot happen under normal circumstances or effectively redirect the reaction to a less favored pathway under thermal conditions.[1] More interestingly, unlike the thermal and photochemical reactions, in which the potential energy surface of the reaction is generally not affected, the mechanical force is believed to distort the original potential energy surface and may therefore result in new reaction patterns.[2] Polymer mechanochemistry is a key component of mechanochemical science, and it focuses on the chemical reactions of polymers under force.[3] Early polymer mechanochemistry involves the treatment of polyalkenes with mechanical force, leading to the homolysis of backbone and generation of fragments with lower molecular weight.[4]

Recently, the focus was diverted to discovering versatile reaction patterns by applying force onto the specific molecules. These specially designed molecules, called mechanophores, are a group of compounds that can easily undergo chemical reactions with loading of a mechanical force.[5] Notably, the mechanophores are usually embedded into long polymer chains to allow the transduction of mechanical force.[3c,5] Owing to the pioneering works in this field, a series of mechanophores were synthesized and subsequently investigated, such as *gem*-dihalocyclopropanes (*g*DHC),[6]

benzocyclobutenes (BCB),[7] spiropyrans (SP)[8] and so forth. The properties of mechanophores, such as the plateau force (i.e., the level of force by which the mechanophore gets activated), can be quantitatively characterized through the SMFS (i.e., Single Molecule Force Spectroscopy) experiments.[9]

Computational methods have also been developed to study the mechanophores.[10] The CoGEF (Constrained Geometry to Simulate External Force) method, which derives the force from a constrained geometry, is widely used nowadays to study the bond rupture under mechanical forces.[11] Although CoGEF is useful in the qualitative discussions of mechanophore reactivity (excluding a few unsuccessful exceptions),[5d] quantitative approaches that can predict the activation force level required to induce chemical bond rearrangements are always desired. There are some such approaches in which force are described explicitly, such as the AISMD (Ab Initio Steered Molecular Dynamics) method developed by Martínez and co-workers[12] and the EFEI (External Force is Explicitly Included) method raised by the Marx group.[13] Recently, the Zimmerman group also suggested a method called SE-GSM (Single-Ended Growing String Method) to study mechanochemical reactions computationally.[14] The term called mechanochemical response index, which is obtained within the framework of conceptual density functional theory, is also used for the description and monitoring of reactions under external force.[15]

The artificial force induced reaction (AFIR) method developed by our group, literally, is to explicitly add an artificial force between certain fragments inside a molecule or a complex to trigger reactions.[16] Normally, the AFIR method employs a force to suppress the potentially interactive atoms or to dissociate a bond so that a reaction can happen, and then, finds a force-free reaction pathway based on the force-induced reaction path.[17] However, from another perspective, we then envisaged, if a repulsion force, F_τ, is added to the certain designated groups of a molecule, it is possible to simulate and predict the chemical outcome of the molecule under stretching force. It is a new route to exploring mechanochemistry computationally. Moreover, unlike the CoGEF method mentioned above, in which the max rupture force is derived from varying the constrained geometry, our AFIR method handles with the force in an explicit way. In this regard, we can observe how the molecule reacts responsively.

We have employed the AFIR method for the latter purpose (i.e., simulating reactions under mechanical force), in our earlier publications to rationalize the experimental observations.[18a,19] In this article, we demonstrate its performance by applying it to a variety of compounds listed in **Figure 1**. We first apply the AFIR method to a variety of mechanophores shown in **Figures 1A**, **1B**, and **1C**, whose activation force levels have already been carefully measured through experiments. The comparison between our calculation results and the experimental data verified the AFIR method as a simple but highly reliable computational tool for the study of mechanochemical reactions under tension. Therefore, the AFIR method is further employed to study a series of practical problems encountered in the current polymer mechanochemistry, such as the force-promoted retro-Diels-Alder

reaction of furan-maleimide adducts shown in **Figure 1D**, the mechanodegradation of generic polymers presented in **Figure 1E** and the degradation of cross-linker molecule (used in the DN-hydrogels) displayed in **Figure 1F**. These computational studies provided useful mechanistic insights which can be used for the further improvement of relevant mechanochemical reactions.
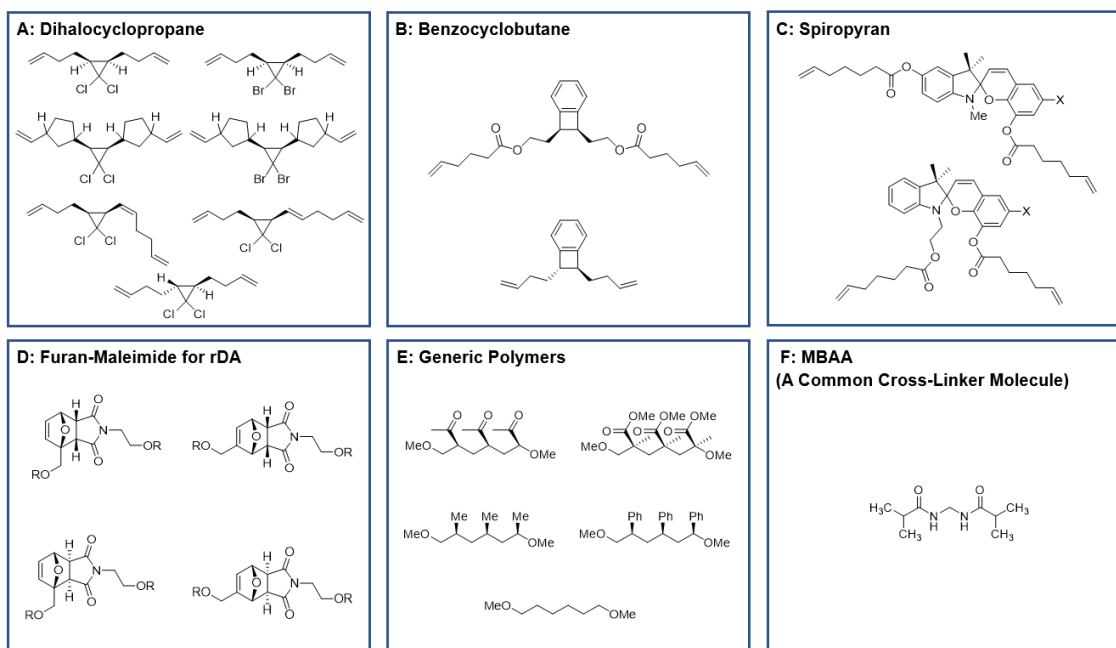

Figure 1. Mechanophores and substrates of mechanochemical reactions subjected to the computational study in this article (**A**: dihalocyclopropanes; **B**: benzocyclobutanes, **C**: spiropyrans; **D**: furan-maleimide substrates for retro-Diels-Alder reactions; **E**: generic polymers for mechanodegradation; **F**: MBAA molecule for force-induced decomposition).

2. Theory

In this study, the AFIR method[16] is employed to simulate the stretching force added to the target molecules. Notably, the AFIR method has been extensively used for the exploration of organic and organocatalytic reactions under normal force-free conditions.[17] The original idea of AFIR is simple, as pushing or pulling two specific intramolecular (or intermolecular) fragments by an artificial force can eventually lead to the reactions. The force is applied to the system by the following AFIR function $F(\mathbf{Q})$.

$$F(\mathbf{Q}) = E(\mathbf{Q}) + \rho\alpha\frac{\sum_{i\in A}\sum_{j\in B}\omega_{ij}r_{ij}}{\sum_{i\in A}\sum_{j\in B}\omega_{ij}} \qquad (1)$$

In Eq. (1), $E(\mathbf{Q})$ is the Born-Oppenheimer potential energy surface (PES) of the given geometrical parameter $\mathbf{Q}$ and the second term applies the force to the system of interest. More specifically, the term α controls the strength of the force added. The parameter ρ can be set to either 1 or -1, of which

the former indicates an attractive force, and the latter leads to a repulsive force. From Eq. (1) we can also notice the force is given as a weighted sum of the interatomic distance r_{ij} between atom i in fragment A and atom j in fragment B, and the weight ω_{ij} is given as follows,

$$\omega_{ij} = \left(\frac{R_i + R_j}{r_{ij}}\right)^6 \tag{2}$$

where R_i and R_j are the covalent radii of atoms i and j, respectively. The force-induced path is optimized to a minimum energy path without mechanical force afterwards. This is done by using a chain-of-states method, such as the locally updated planes (LUP)[20] method, to find an actual force-free reaction path. In our cases, an in-house-modified LUP method is used in the implementation.[16]

What makes this work different from the other AFIR calculations is that two types of forces are used in this work, of which one is the genuine force that the polymer feels, while the other is the artificial force same as the one in the usual AFIR calculations. First, we use the AFIR function to construct the force-modified potential surface (i.e., FMPES) $E^{FM}(\mathbf{Q})$, on which the second set of artificial force used to cleave covalent bonds is then added.

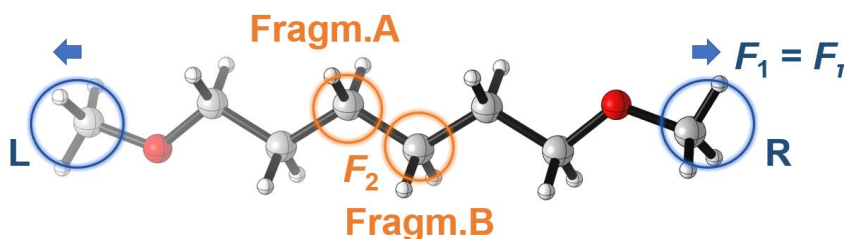**Figure 2.** Two types of forces used in our AFIR calculations, where τ represents the strength of the genuine force that the polymer feels, **L** is the left-hand side terminal group, **R** is the right-hand side terminal group, **A** and **B** are fragments that are pushed or pulled in the AFIR procedure to induce a reaction, and the other parameters, ω, r, ρ, and α, are identical to those in equations 1 and 2.

More specifically, as shown in **Figure 2**, a repulsive force F_τ with a strength of τ is added to the termini of the molecule of interest (labeled as **L** and **R**), which therefore turns to be a stretching force and helps to construct the FMPES $E^{FM}(\mathbf{Q})$. The mathematical formula of $E^{FM}(\mathbf{Q})$ is shown in Eq. (3).

$$E^{FM}(\mathbf{Q}) = E(\mathbf{Q}) - \tau \frac{\sum_{i \in L} \sum_{j \in R} \omega_{ij} r_{ij}}{\sum_{i \in L} \sum_{j \in R} \omega_{ij}} \tag{3}$$

Please note that the force was added to the designated groups, rather than two single atoms, which therefore prevents some unwanted transformations (such as conformation change or even C-H cleavage) at the terminal groups when large force is added. It is also noteworthy that the computation of the force-coupled barrier $\Delta G^{\ddagger}_\tau$ is based on this FMPES, $E^{FM}(\mathbf{Q})$. Meanwhile, as what is shown in Eq. (4), another set of artificial force F_2, of which the strength and direction is controlled by ρ and α,

is added to the system.

$$F(\mathbf{Q}) = E^{\text{FM}}(\mathbf{Q}) + \rho\alpha\frac{\sum_{i\in A}\sum_{j\in B}\omega_{ij}r_{ij}}{\sum_{i\in A}\sum_{j\in B}\omega_{ij}} \tag{4}$$

It should be emphasized that the latter force F_2 is a purely artificial force to trigger chemical reactions. It is used for finding a possible reaction path and is finally eliminated, being same as the usual AFIR calculations. Here, this is the first time we used two types of forces simultaneously in our AFIR calculations, and it enables us to explore the mechanochemical reactions of any covalent bonds of interest in the system.

3.   Results and discussion

As what was mentioned previously, we envisaged that the AFIR method can be used as a simple but effective tool to study the mechanochemical reactions in a quantitatively correct manner. Therefore, to test such a hypothesis, we decided to first use it for the computational exploration of a series of known mechanophores whose activation data have been measured experimentally, which include *gem*-dihalocyclopropane, benzocyclobutane and spiropyran. It is noteworthy that each of them has some distinctive features as a mechanophore. More specifically, for example, the reactivity of *gem*-dihalocyclopropane can be adjusted by changing the halogen atom and the polymer chain. The spiropyran chosen in our computational study was reported to have an extraordinarily low activation force (~ 300 pN). The mechanochemical reaction of benzocyclobutane is a vivid example that breaks the conventional Woodword-Hoffmann rules. A comparison will be made between the experimental data and our computational results to demonstrate the accuracy of the AFIR method in handling with these mechanochemical reactions. Moreover, our computational work helps to reveal new mechanistic information for these known mechanochemical reactions. Once it is realized that the AFIR method can deliver the activation data quantitatively consistent to the SMFS data, we then employed the AFIR method to solve the practical problems encountered in current research, such as the force-triggered retro-Diels-Alder reaction, the mechanodegradation of commercially available polymers and the force-promoted decomposition of cross-linker molecules used in DN-hydrogels. Please note that there is currently no SMFS data for the above-mentioned three types of reactions, which means that the calculation results are helpful to the further study in this field.

Note that the activation tensile force required to cause a bond activation under a given condition (temperature T in kelvin and timescale t in second) is denoted as $F_{\text{act}[T,\,t]}$, together with an indication whether the value is obtained experimentally (i.e., $F_{\text{act}[T,\,t],\text{exp}}$) or computationally (i.e., $F_{\text{act}[T,\,t],\text{calc}}$). The computational timescale corresponds to the half-life time estimated by the Eyring equation, using an activation Gibbs energy barrier under a given condition obtained on the FMPES. The common assumptions, such as the standard ideal gas, rigid rotor, and harmonic approximations, are also employed. Similarly, the (overall) Gibbs energy barrier $\Delta G^{\ddagger}_{\text{act}}$ and rate constant k_{act} for the bond

activation under a given condition (temperature T in kelvin and tensile force τ in pico-Newton) are denoted as $\Delta G^{\ddagger}_{\text{act}[T, \tau]}$ and $k_{\text{act}[T, \tau]}$, respectively, with the indication either "exp" or "calc."

Gem-dihalocyclopropane system. Our study first focused on a variety of *gem*-DHC (*gem*-dihalocyclopropane) molecules which have been synthesized and examined experimentally. The experimental data reported can be used for the evaluation of our calculation accuracy.[6,21] Shown in **Figure 3** is the model molecule used in our initial calculations. Literally it is the *gem*-DCC (*gem*-dichlorocyclopropane) embedded in *Z*-polybutadiene chain, and it is therefore named *g*DCC_PB. The initial calculation conducted is called the MIN calculation, which is to fully optimize the force modified potential energy surface $E^{\text{FM}}(\mathbf{Q})$ (i.e., taking the simulated tensile force F_τ as the constraint while doing minimization calculations). As what can be seen from **Figure 3**, the repulsive force F_τ is added between two methylene groups (CH_2) at the terminal positions by setting them as **L** and **R** in Eq. (3) to simulate the stretching force. Therefore, the minimization with the force F_τ as a constraint shows a vivid image of how the molecule acts responsively with the external tensile force.
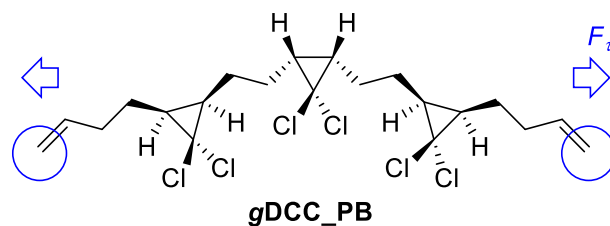

Figure 3. Mechanophore *g*DCC_PB on which the tensile force F_τ is applied.

Shown in **Figure 4** is the force-extension curve generated by the AFIR method. The value of the extension is defined as the difference between the polymer chain lengths at $F_\tau = x$ pN and $F_\tau = 0$ pN (i.e., using the force-free polymer chain length as the reference). Each dot in the figure represents an MIN calculation at the given tensile force F_τ. The curve shown in the figure can be easily divided into four regions. The first region is where the twisted polymer gets decoiled and adopts a straight *zig-zag* conformation. It is known that the polymer stays twisted under force-free condition (i.e., $F_\tau = 0$ pN), because of the effect of an entropy increase. In our calculation, we only considered part of the entire polymer chain and there is no large-scale conformational rearrangement. Therefore, such a conformational change is relatively easy in the model calculation. When a small force F_τ is applied, the conformation of the polymer quickly turns straight and the distance between two termini can be approximately regarded as the contour length of this polymer chain. In **Figure 4**, it could be noticed that, once the polymer is fully extended to reach its contour length, the further increasing of the end-to-end distance then becomes difficult, as it is now to deviate the C-C bond from its equilibrium position. With the gradually increasing stretching force F_τ, the scissible C-C bond is further stretched and finally breaks at a certain level of force. Since there are three *g*DCC units embedded in the same

polybutadiene scaffold, the almost simultaneous C-C cleavage results in an instant and significant increase of the polymer length. Such a phenomenon can also be seen in the real SMFS experiments, and it is named signature plateau.[6c] Once the incorporated mechanophores have all been activated, the force F_τ at a higher level will further stretch the backbone of the product until the final rupture of the backbone. This can be seen as the fourth region of the curve shown in **Figure 4**. In this case, for the gDCC_PB, the plateau force was found as 3500 ~ 3700 pN, which indicates the C-C bond in the cyclopropane moiety will be cleaved at the timescale of 0 second when the external tensile force F_τ reaches this level. The simple MIN calculation using the AFIR method to simulate the external force therefore offers us a straightforward way to observe how the mechanophore reacts under a stretching force from the computational perspective. However, it must be emphasized that the activation force predicted by the MIN calculation is the force needed to break the scissible bond at the timescale of 0 second and the temperature of 0 kelvin (i.e., $F_{\text{act}[T=0\text{ K}, t=0\text{ s}],\text{calc}}$). That is why this value (3500 ~ 3700 pN) is much larger than the actual activation force ($F_{\text{act}[T=298.15\text{ K}, t=0.1\text{ s}],\text{exp}}$ ~ 1330 pN) recorded in the SMFS experiment.[6c]
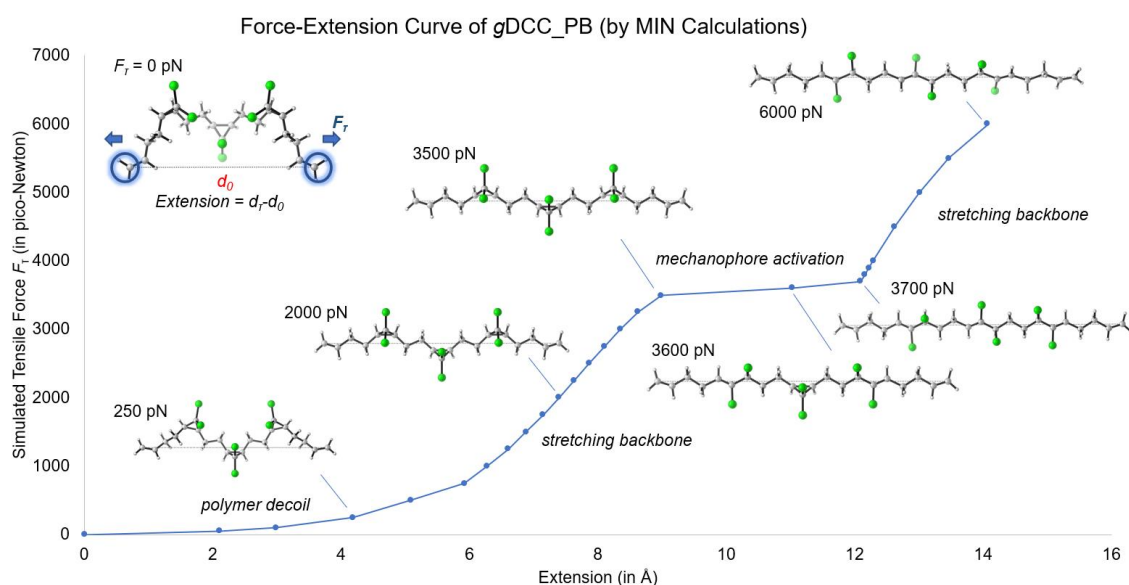

Figure 4. Force-Extension (the distance between the terminal C atoms in Å) curve of gDCC_PB trimer generated through the MIN calculation of the FMPES in Eq. (3) (method: B3LYP-D3/6-311G(d,p)), from which we can observe four regions and the geometry change at the signature plateau region.

In fact, each SMFS measurement has a certain timescale and is conducted at room temperature. If we consider the timescale of the reaction, the real activation force level $F_{\text{act}[T, t]}$ should be much lower. However, this requires us to obtain the free energy barrier of the mechanochemical reaction under external force. In fact, with the assistance of the AFIR which provides the FMPES, we can locate the

transition state of the expected reaction at any given F_τ. The data collected can be subsequently fitted to a curve that correlates the force-coupled free energy barrier $\Delta G^{\ddagger}_\tau$ and the force level F_τ. Based on such a curve, we are able to make a computational prediction of the activation force level $F_{\text{act}[T,\ t],\text{calc}}$, given the timescale of the experiment.
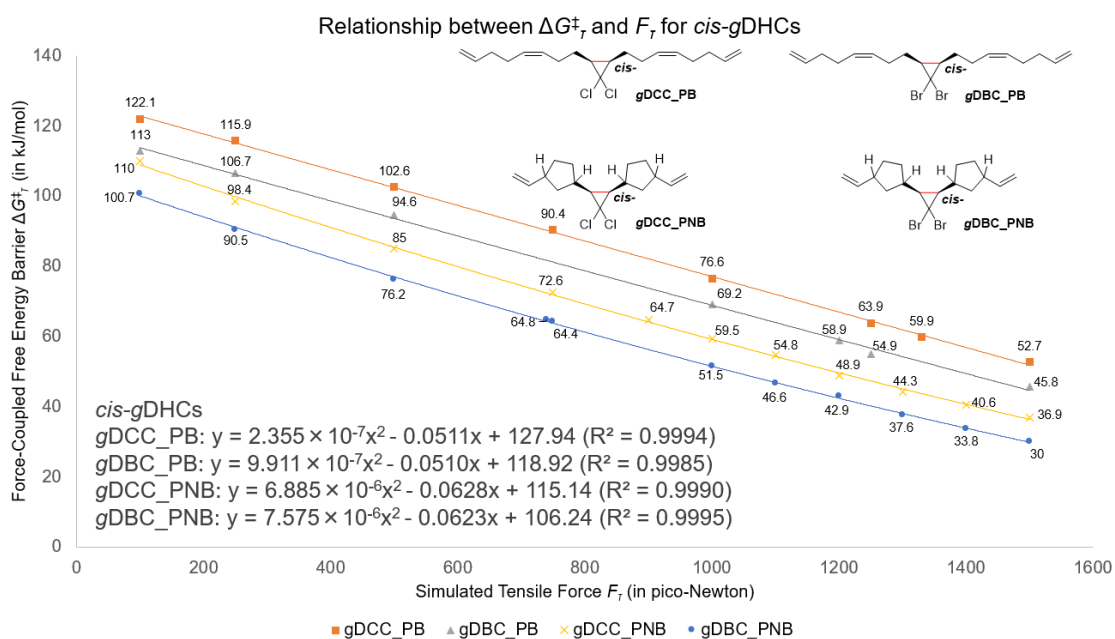

Figure 5. Fitting curves that depict the relationship between the force-coupled Gibbs energy barrier $\Delta G^{\ddagger}_\tau$ and the level of tensile force F_τ for *g*DCC_PB, *g*DBC_PB, *g*DCC_PNB and *g*DBC_PNB. Here PB means polybutadiene backbone and PNB represents polynorbornene backbone.

Shown in **Figure 5** is the $\Delta G^{\ddagger}_\tau - F_\tau$ graph for a series of *g*DHCs. Each dot in the figure represents a transition state optimization calculation on the FMPES. It is clear from the figure that the free energy barrier $\Delta G^{\ddagger}_\tau$ of the C-C cleavage process decreases with an increasing level of external force F_τ. More specifically, a simple model derived from the Marcus theory[22] suggests that the barrier decreases as a quadratic function of the force level F_τ (please see SI for the derivation process). Therefore, this study represents the $\Delta G^{\ddagger}_\tau - F_\tau$ curves with a quadratic function. Inspection on the four curves shows the reactivity of four *g*DHCs under the same level of F_τ is: *g*DBC_PNB > *g*DCC_PNB > *g*DBC_PB > *g*DCC_PB, being consistent with the experimental observations reported by Craig and co-workers.[6c] Moreover, since the SMFS test which derives the activation force was conducted at the timescale of 0.1 s, the force-coupled free energy barrier $\Delta G^{\ddagger}_{\text{act}[T\ =\ 298.15K,\ \tau],\text{calc}}$ should be around +68.2 kJ·mol^{-1}, according to the Eyring equation (i.e., corresponding to a half-life time of 0.1 s at 298.15 K). Given this, the computed activation forces $F_{\text{act}[T\ =\ 298.15\ K,\ t\ =\ 0.1\ s],\text{calc}}$ for *g*DCC_PB, *g*DBC_PB, *g*DCC_PNB and *g*DBC_PNB are 1180 pN, 1010 pN, 820 pN and 660 pN, respectively. It is noteworthy these

calculated activation force levels are very close to those reported experimentally, as what can be seen from **Table 1**.

Besides the calculations concentrating on the halogen and backbone effects, we also employed the AFIR method to study the stereo-effect which was reported to affect the activation force level as well. The Craig group has reported that *trans-g*DCC has a much larger activation force than its *cis*-isomer.[23] The experimental data $F_{\text{act}[T = 298.15 \text{ K}, t = 0.1 \text{ s}],\text{exp}}$ and our computed result $F_{\text{act}[T = 298.15 \text{ K}, t = 0.1 \text{ s}],\text{calc}}$ for *trans-g*DCC are 2290 and 2230 pN respectively, which are also very close.
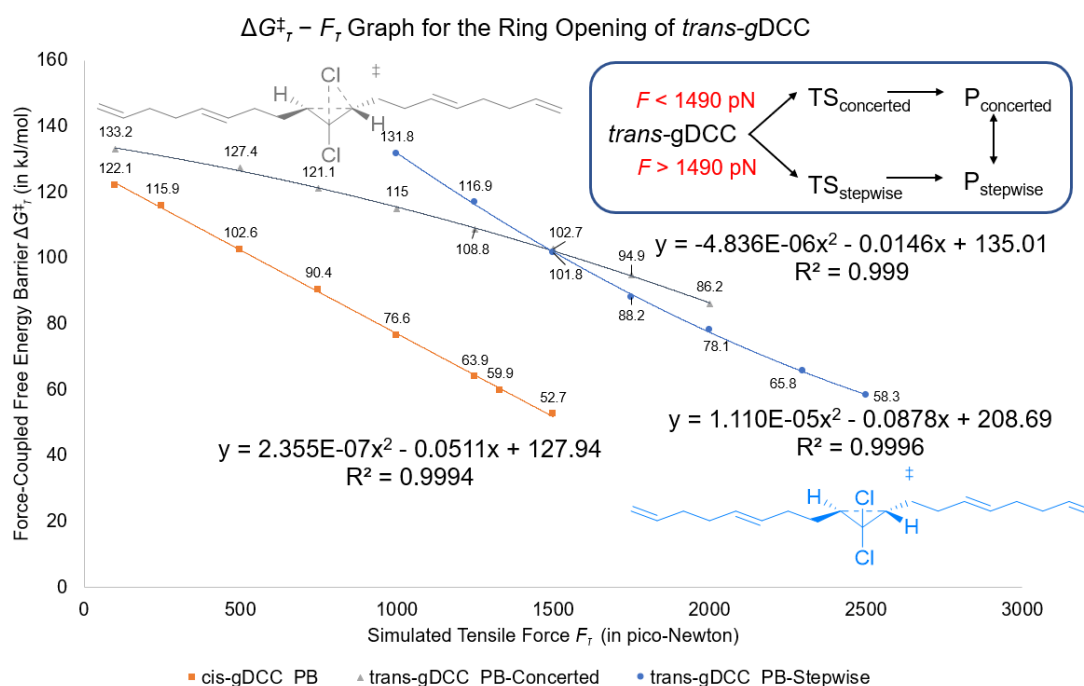

Figure 6. $\Delta G^{\ddagger}_{\tau} - F_{\tau}$ graph for *trans-g*DCC_PB (from which we can clearly see the concerted transition state is more energetically favored at low force-level region and the stepwise transition state is predominant at high force-level region)

Very interestingly, our calculations helped to locate two different transition states for *trans-g*DCC, including a concerted transition state and a stepwise one, of which the latter first leads to a diradical intermediate. The concerted transition state (marked in grey color in **Figure 6**), in which the transfer of chloride and the C-C breaking happen simultaneously, has a much lower free energy barrier at low force-level region (i.e., with a small F_{τ}). However, the stepwise transition state becomes predominate once the force F_{τ} is over 1490 pN. Thus, for *trans-g*DCC, it actually undergoes a stepwise transition state for its activation (please refer to the SI for the IRC curves of these two transition states).

It was also found experimentally that, a C=C double bond, if directly attached to the cyclopropane ring, can lead to the ring-opening reaction at a relatively lower force.[21] Moreover, the stereochemistry

of the alkene moiety also plays a vital role in lowering the activation force $F_{\text{act}[T = 298.15 \text{ K}, t = 0.1 \text{ s}],\text{exp}}$. Compared to the C=C double bond in *Z*-configuration, the *E*-alkene moiety can significantly bring down the activation force $F_{\text{act}[T = 298.15 \text{ K}, t = 0.1 \text{ s}],\text{exp}}$ to the level of 800 pN. The AFIR calculations simulating the ring-opening reaction of these two *gem*-DCC species were carried out and the results are also shown in **Table 1**. Despite the semi-quantitatively correct data that reproduced the experimental activation force levels, our calculation also found that, both *g*DCC_DBE and *g*DCC_DBZ have similar intrinsic reactivity. That is to say, the breaking C-C bonds in both compounds are similarly strong under force-free conditions (i.e., $F_\tau = 0$ pN). Regarding this statement, it can be verified if we inspect the low-force region of the $\Delta G^{\ddagger}_\tau - F_\tau$ graph. When $F_\tau = 100.0$ pN (i.e., low-force region, see **Figure S3** in SI), the computed Gibbs energy barriers of the ring-opening reaction are +91.0 and +94.4 kJ·mol^{-1} for *g*DCC_DBE and *g*DCC_DBZ, respectively. The higher reactivity of *g*DCC_DBE under tensile force F_τ, is due to its stronger sensitivity towards the external force, as what can be confirmed by the much steeper slope of its $\Delta G^{\ddagger}_\tau - F_\tau$ curve. Therefore, the double bond in *E*-configuration, can be regarded as a motif that enhances the force effect.

Table 1. Experimental and computed activation forces $F_{\text{act}[T = 298.15 \text{ K}, t = 0.1 \text{ s}]}$ of various *gem*-DHCs

*g*DCC_PB

*g*DBC_PB

*g*DCC_PNB

*g*DBC_PNB

*trans-g*DCC_PB

*g*DCC_DBE

*g*DCC_DBZ
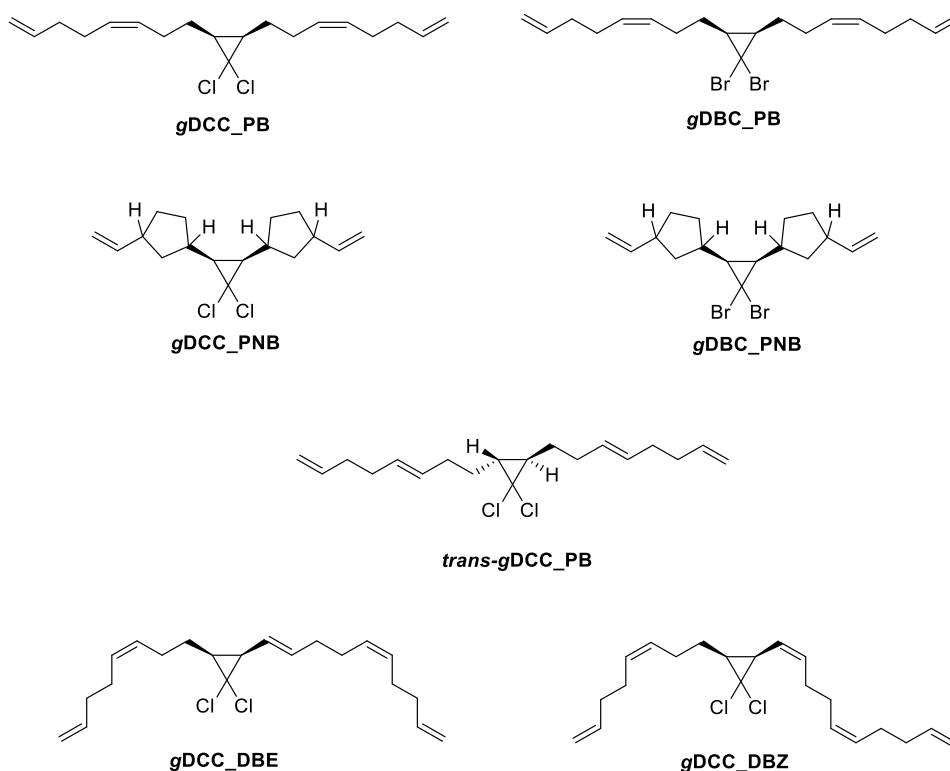
Species	$F_{\text{act}[T = 298.15 \text{ K}, t = 0.1 \text{ s}],\text{exp}}$	$F_{\text{act}[T = 298.15 \text{ K}, t = 0.1 \text{ s}],\text{calc}}$
*g*DCC_PB	1330	1180
*g*DBC_PB	1200	1010
*g*DCC_PNB	900	820
*g*DBC_PNB	740	660
*trans-g*DCC_PB	2290	2230
*g*DCC_DBE	800	550
*g*DCC_DBZ	1160	870

Spiropyran system. Having confirmed that our AFIR method can reproduce both qualitative and semi-quantitatively correct data for the *gem*-dihalocyclopropane system, we then turned our focus to another famous mechanophore, the spiropyran. Compared to the *gem*-DHC system, spiropyrans are much more reactive under external force. The ring-opening reaction can be activated with an extraordinarily low force as low as 300 pN.[8b] In addition, the sensitivity of spiropyrans towards external force F_τ can be easily manipulated by changing the position of two polymer arms or switching the substituent group on the benzene ring where the C-O bond locates. Given this, to further test the broad availability of our AFIR method, we performed calculations on the spiropyran system. The spiropyran SP1 was reportedly less reactive than SP2.[8b,8d] Shown in **Figure 7** are the transition states

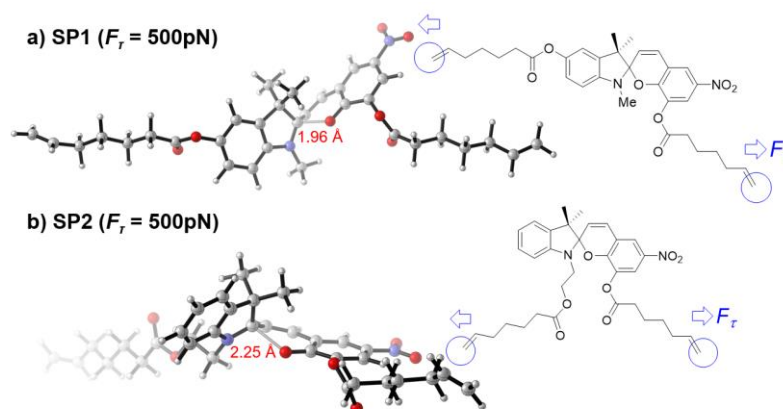of ring-opening process for both SP1 and SP2 at $F_\tau = 500$ pN.

Figure 7. Optimized geometries of the transition states linked to the ring-opening reaction for SP1 and SP2 with $F_\tau = 500$ pN.

The force-coupled free energy barriers associated with these two transition states are +52.4 and +25.6 kJ·mol^{-1}, respectively. It clearly indicates that SP2 is much more reactive under the same level of external force F_τ. To furnish the ring-opening reaction at the timescale of 0.1 s (which connects to a Gibbs energy barrier around 68.2 kJ·mol^{-1}), the computed activation force level $F_{\text{act}[T = 298.15 \text{ K}, t = 0.1 \text{ s}],\text{calc}}$ is indeed lower than 500 pN. Our calculations also showed that, the open-ring product is in fact thermodynamically less stable. An *s-cis* to *s-trans* isomerization of the newly formed butadiene moiety happens straightaway after the ring-opening step, affording a more stable merocyanine isomer (see the SI for details).

Our later efforts were made to reproduce the substituent effect observed experimentally. The force-coupled rate constants $k_{\text{act}[T, \tau],\text{exp}}$ for a series of SP2 molecules were carefully measured and reported by Craig and co-workers.[8c] Based on the Eyring equation, the rate constant $k_{\text{act}[T, \tau],\text{exp}}$ can be readily transformed to the force-coupled Gibbs energy barrier as shown in **Table 2**. We also carried out calculations using the AFIR method to provide a tensile force F_τ of 375.0 pN for three different SP2 molecules, named SP2_H, SP2_Br and SP2_NO2. The transition states of C-O cleavage under a constraint F_τ of 375.0 pN force were successfully located and the force-coupled free energy barriers $\Delta G^{\ddagger}_\tau$ were computed. The computed data is shown in **Table 2**, from which SP2_NO2 was found most reactive and then it comes SP2_Br. The unsubstituted SP2_H, is the least reactive. Note that the process consists of two steps, i.e., C-O cleavage and *s-cis* to *s-trans* isomerization, and **Table 2** presents the overall barriers that corresponds to the Gibbs free energy gap between the highest transition state and the reactant (see SI for more details).

Table 2. Substituent effect on the ring-opening reaction of spiropyran SP2 at F_τ = 375 pN (breaking bonds are highlighted in red).
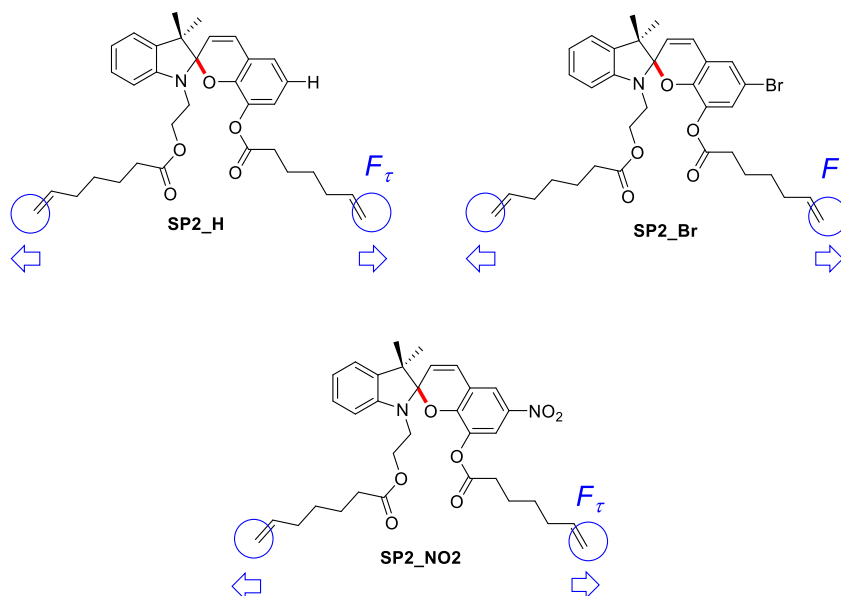

Species	$\Delta G^\ddagger_{\text{act}[T = 298.15 \text{ K}, \tau = 375 \text{ pN}],\text{exp}}$ [a]	$\Delta G^\ddagger_{\text{act}[T = 298.15 \text{ K}, 375 \text{ pN}],\text{calc}}$
SP2_H	+67.5 kJ·mol⁻¹	+51.8 kJ·mol⁻¹
SP2_Br	+64.6 kJ·mol⁻¹	+49.2 kJ·mol⁻¹
SP2_NO2	+54.7 kJ·mol⁻¹	+43.1 kJ·mol⁻¹

[a] Obtained by transforming $k_{\text{act}[T = 298.15 \text{ K}, \tau = 375 \text{ pN}],\text{exp}}$ (= 9.0, 32.0, and 1600.0 s⁻¹, respectively, for SP2_H, SP2_Br, and SP2_NO2)[8c] via the Eyring equation.

Benzocyclobutane system. Another famous mechanophore, the benzocyclobutane system (BCB), was also revisited by our AFIR method. The ring-opening of *cis*-BCB under mechanical force was confirmed as a vivid case that violates the Woodward-Hoffmann rules. Furthermore, the thermally inert *cis*-isomer was found having a smaller activation force $F_{\text{act}[T = 298.15 \text{ K}, t = 0.1 \text{ s}],\text{exp}}$ (i.e., being more reactive), if compared to the *trans*-isomer, according to the experimental observations.[23] Being consistent to the experimental data, our calculations also suggest that the *cis*-isomer (*cis*-BCB) is more reactive than the *trans*-isomer (*trans*-BCB), of which the computed activation forces $F_{\text{act}[T = 298.15 \text{ K}, t = 0.1 \text{ s}],\text{calc}}$ are 1430 pN and 1620 pN. Shown in **Table 3**, our calculation results do not only correctly predict the order of reactivity for these two BCB molecules under external force, but also reproduce the quantitatively consistent activation force level with an error less than ~ 120 pN. Interestingly, we also found that the disrotatory ring opening reaction is not favored for the *cis*-BCB at low-force region, as the slope of the fitting curve of *cis*-BCB is much steeper than that of the *trans*-BCB (see **Figure S8** for more details). It therefore indicates that the ring-opening reaction should follow the Woodward-Hoffmann rules under force-free conditions, which is exactly what can be seen experimentally.

Table 3. Experimental and computed activation forces $F_{\text{act}[T = 298.15\text{ K}, t = 0.1\text{ s}]}$ for two benzocyclobutanes
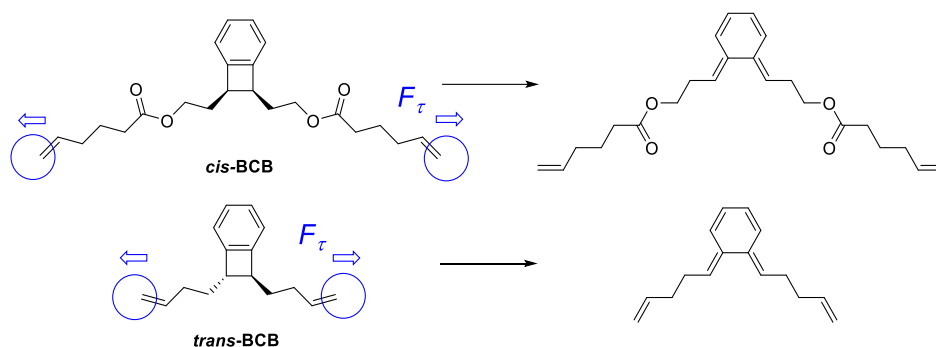
Species	$F_{\text{act}[T = 298.15\text{ K}, t = 0.1\text{ s}],\text{exp}}$	$F_{\text{act}[T = 298.15\text{ K}, t = 0.1\text{ s}],\text{calc}}$
cis-BCB	1370	1430
trans-BCB	1500	1620

Force-triggered retro-Diels-Alder reactions. The Diels-Alder reaction is a one of the most famous pericyclic reactions leading to the formation of a stereospecific six-member ring simply from a diene and a substituted alkene (i.e., dienophile).[24] Due to the simplicity of the reactants and the complexity of the products it leads to, it therefore serves as a powerful and reliable tool in organic synthesis.[25] It should be noted that the Diels-Alder reaction is less reversible under low temperatures. Nevertheless, recently, De Bo and co-workers revealed that the retro-Diels-Alder reaction, can be realized with the assistance of mechanical force even at low temperatures (5–10 °C).[26a] It was also found that the geometry of the Diels-Alder adduct strongly affects its reactivity.[26] Shown in **Figure 8** are the four furan-maleimide Diels-Alder adduct compounds subjected to the force-triggered retro-Diels-Alder reaction.
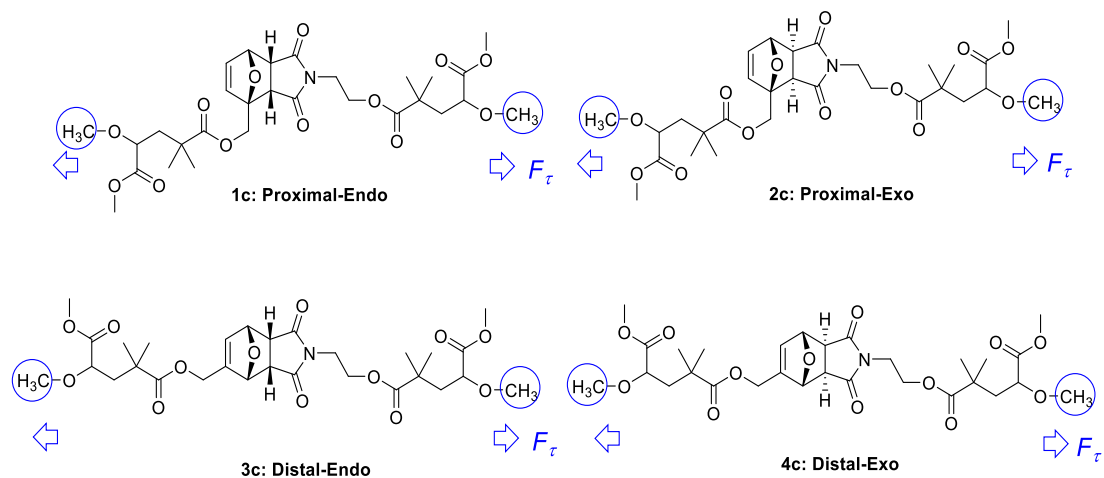
Figure 8. Furan-maleimide Diels-Alder adducts subjected to tensile force.

We noted that De Bo and co-workers have shared their computational studies on the mechanism of retro-Diels Alder reaction[27] using the EFEI method.[13] They highlighted that the external force F_τ helps to transform the concerted transition state to a stepwise one. For compounds **1c**, **2c** and **3c**, such a critical force is around 1.0 nN while it is 2.4 nN for compound **4c**. Here, we also would like to explore this force-promoted retro-Diels-Alder reaction using the AFIR method, aiming at providing a prediction of the activation forces $F_{\text{act}[T = 298.15 \text{ K}, t = 0.1 \text{ s}],\text{calc}}$, which are currently unavailable experimentally. In our case, a repulsive force F_τ is directly added to the two terminal -CH$_3$ groups (see **Figure 8**). The optimization to find minima and transition states was with this force constraint. A set of forces F_τ were eventually tested and the force-coupled free energy barrier under each force level ($\Delta G^{\ddagger}_\tau$) was successfully obtained for all four isomers (see **Figure 9** for the details).
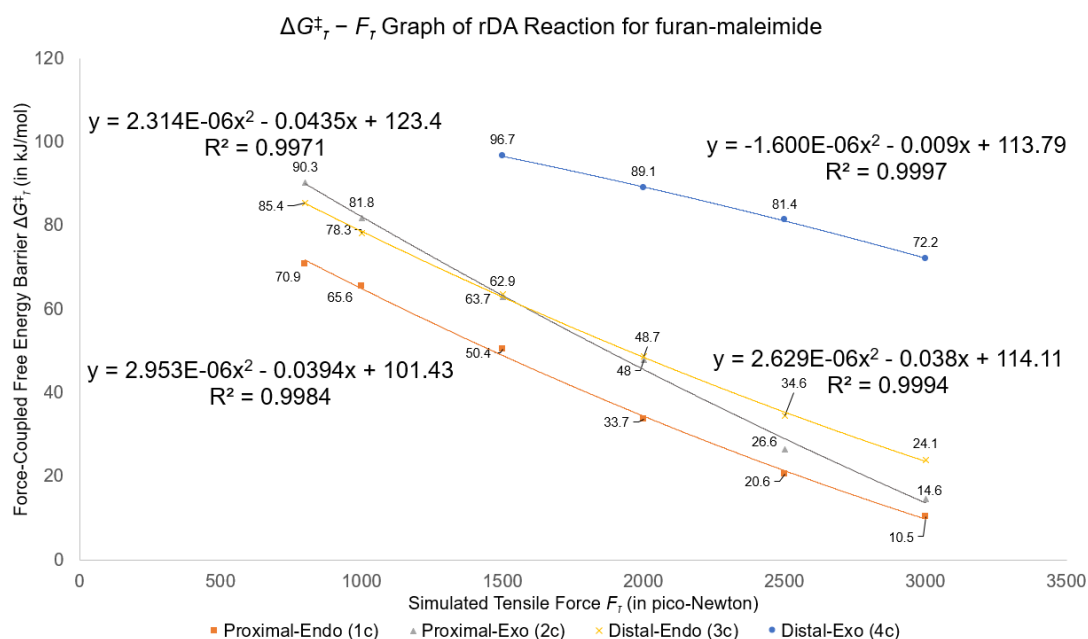
Figure 9. Effect of stretching force F_τ on the force-coupled free energy barrier $\Delta G^{\ddagger}_\tau$ of retro-Diels-Alder reaction for furan-maleimide.

Gratifyingly, in our AFIR exploration, it is also confirmed that Distal-Exo (**4c**) is the most force-resistant compound. Even at F_τ = 3000 pN, the barrier $\Delta G^{\ddagger}_\tau$ is still up to +72.2 kJ·mol^{-1}. However, the retro-Diels-Alder reaction for the other three isomers (**1c**, **2c** and **3c**) are almost barrierless with a tensile force F_τ of 3000 pN, being +10.5, +14.6 and 24.1 kJ·mol^{-1}, respectively. Though the SMFS data for this set of compounds is not available till now, based on the $\Delta G^{\ddagger}_\tau - F_\tau$ relationship concluded in **Figure 9**, we can predict the activation force $F_{\text{act}[T = 298.15\text{ K}, t = 0.1\text{ s}],\text{calc}}$ for **1c** (Proximal-Endo), **2c** (Proximal-Exo), **3c** (Distal-Endo) and **4c** (Distal-Exo) as 900 pN, 1370 pN, 1330 pN and 3220 pN. Therefore, Diels-Alder adduct compounds **1c**, **2c** and **3c** are qualified mechanophores. Meanwhile, we believe the SMFS data for **4c** will be difficult to obtain due to the extremely large activation force required. From the generated $\Delta G^{\ddagger}_\tau - F_\tau$ graph, it is also noteworthy that compound **2c** is much more sensitive to the external force if compared to **3c**. At high force region, **2c** is more reactive than **3c**, while it is more inert than **3c** if F_τ is lower than 1550 pN. It is consistent to the experimental data that **3c** is more reactive than **2c** under thermal conditions.
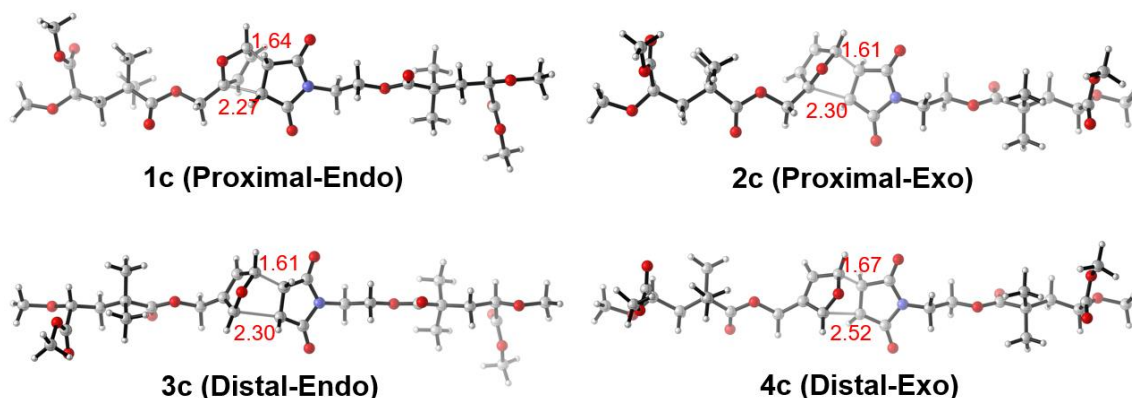
Figure 10. Optimized transition state geometries for all four isomers at $F_\tau = 2000$ pN

Shown in **Figure 10** are the transition states of all four isomer at $F_\tau = 2000$ pN. Similar to what De Bo and co-workers have indicated,[27] the external force greatly affects the geometry of transition states, resulting in unequally long C-C bonds which are prone to break (see SI for the detailed table of C-C bonds at transition state under different F_τ). For example, in **1c** (Proximal-Endo), these two C-C bonds are 2.27 Å and 1.64 Å long, respectively. The C-C bond, which has the tensile force directly passing through, extends much longer and breaks first. The stepwise transition state is defined based on the bonding rather than the energy. According to the IRC calculations, in fact, there is no intermediate showing up after the first C-C bond breaks on the FMPES $E^{FM}(\mathbf{Q})$. By AFIR method, we also confirmed there is a certain threshold for the special stepwise transition state switching to the conventional concerted transition state with equally long C-C bonds. For **1c** and **2c**, the force level is around 500 pN, while it is around 200 pN for **3c**. For compound **4c**, the switching point comes much earlier as the critical force is around 1000 pN. Please refer to the SI for the details.
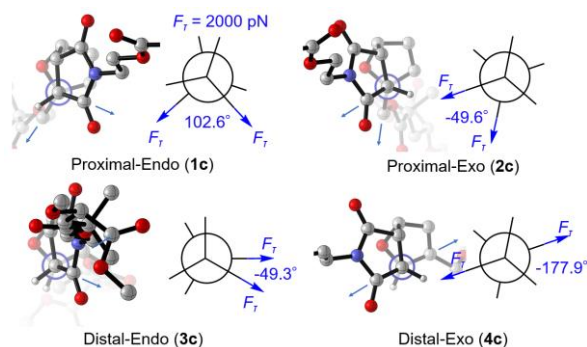

Figure 11. Illustration of "node" along the transduction path of force F_τ.

Further inspections on the geometries suggest that all the reactive isomers have a "node" at the breaking C-C bond. Regarding the definition of node, careful inspections on the structural motif shown

in **Figure 11** suggest that, if we take the Newman projections concerning the breaking C-C bond, we will find the angle between two stretching forces is less than or around 90°. It can be seen in the cases of **1c** (Proximal-Endo), **2c** (Proximal-Exo) and **3c** (Distal-Endo). However, the pair of tensile forces are parallel in **4c** (Distal-Exo) and the angle is around 180°. We believe such a node inhibits the transduction of tensile force and is supposed to generate a torque on the bond prone to break first. In the most force-resistant isomer **4c** (Distal-Exo), such a node does not exist, and the tensile force can pass freely through the breaking C-C bond without any hindrance. The computational study on the retro-Diels-Alder reaction shows a vivid example that how a specially designed geometry can significantly amplify the effect of mechanical force. The structural information (i.e., "nodes" on the transduction direction of force) revealed by the AFIR calculations can be used for the further enhancement of force-responsive ability, even for those less reactive compounds.

Mechanodegradation of generic polymers. The degradation of plastic wastes is always a challenging work and meanwhile remains as a hot topic in modern society as the plastic wastes possess a significant threat to the environment.[28] Compared to the thermal oxidation pathway,[29] the mechanodegradation is an eco-friendlier approach. Dated back to 1930s, Staudinger reported the first case of mechanodegradation of plastic as he found that the molecular weight of polystyrene decreased if treated with mechanical force.[4] It was then experimentally realized that generic polymers can be degraded smoothly under the force provided by ball milling.[3a,18] The force-promoted decomposition of polymers involves the homolytic cleavage of covalent bonds, and the mechanoradicals generated from this process have been detected and characterized by ESR (i.e., electron spin resonance) method experimentally.[30] However, to the best of our knowledge, so far, there is no detailed computational chemistry report for the feasibility of generic polymers towards the mechanodegradation process. Experimentally, it is difficult to employ the conventional SMFS experiments for the measurements of rupture forces $F_{\text{act}[T, t],\text{exp}}$ of generic polymers, since most of them possess a considerably large $F_{\text{act}[T, t],\text{exp}}$ (which will result in the detachment of sample from the tip of AFM (atomic force microscopy)). Given this challenge, the AFIR method was used to systematically study the mechanodegradation process of a series of commercially available polymers, from which we would like to obtain the quantitative data of rupture forces. We also would like to acquire the useful structure-reactivity information from the calculations, such as how the nature of covalent bond and the substituent effect affect $F_{\text{act}[T, t]}$.

The polymers chosen for our computational study are shown in **Figure 12**. They were firstly categorized into three main groups: polymers with carbonyl substituents (e.g., PMMA and PMVK), polyalkenes (e.g., PE, PS and PP), and polymers with C-S bonds embedded in the main chain (e.g., PPS and PSU). Given the stereochemistry of polymers, please note that we first studied the isotactic polymers and then the syndiotactic ones. Considering the computational details, we used a trimer molecule as the model molecule for our calculations. Meanwhile, the methoxy group -OMe, was

assigned to all the model molecules as the end-group found in real polymers. A repulsive force F_τ, realized by the AFIR method, was added to these two methyl groups. Such a repulsive force F_τ therefore acts as a tensile force that stretches the polymer chain.
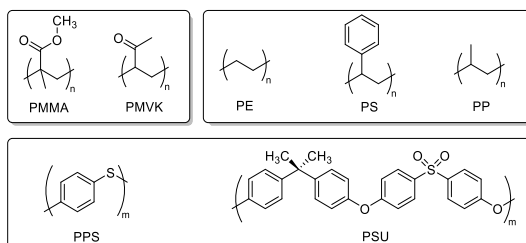

Figure 12. Generic polymers subjected to the computational study

The transition states of covalent bond homolysis under a variety of force levels were successfully obtained and the data (including the force level F_τ and the force-coupled Gibbs energy barrier $\Delta G^{\ddagger}_\tau$) was subsequently used for the curve-fitting. **Figure 13** shows the $\Delta G^{\ddagger}_\tau - F_\tau$ curve of the isotactic PMMA, from which we can clearly see $\Delta G^{\ddagger}_\tau$ of the C-C homolytic cleavage is quadratically dependent on the tensile force F_τ. The force-coupled Gibbs energy barrier gradually decreases with an increasing F_τ starting from 1000 pN. Once the stretching force F_τ reaches 4000 pN, the Gibbs energy barrier of the C-C homolysis in isotactic PMMA drops to only +25.2 kJ·mol^{-1}, suggesting an instant reaction under room temperature. With the $\Delta G^{\ddagger}_\tau - F_\tau$ graph in hand, the rupture force $F_{act[T = 298.15 \text{ K}, t = 654 \text{ s}],calc}$ of isotactic PMMA can be easily computed, which is around 2400 pN. Please note that here we use $\Delta G^{\ddagger}_\tau$ of 90 kJ·mol^{-1} (i.e., $t_{1/2} \sim 654$ s) as the threshold to determine the activation force, since the timescale of the polymer degradation is much larger than that of the common SMFS experiments (usually ~ 0.1 s). Further inspection on the optimized transition state under different level of forces indicates the tensile force F_τ promotes an early transition state. The distance of the breaking C-C bond at transition state strongly depends on the level of F_τ. When F_τ reaches 4000 pN, the C-C distance is 2.39 Å. The C-C distance gradually extends with a decreasing force. When F_τ is 1000 pN, the C-C distance in the transition state becomes 2.78 Å (see **Figure S13** in the SI for more details).
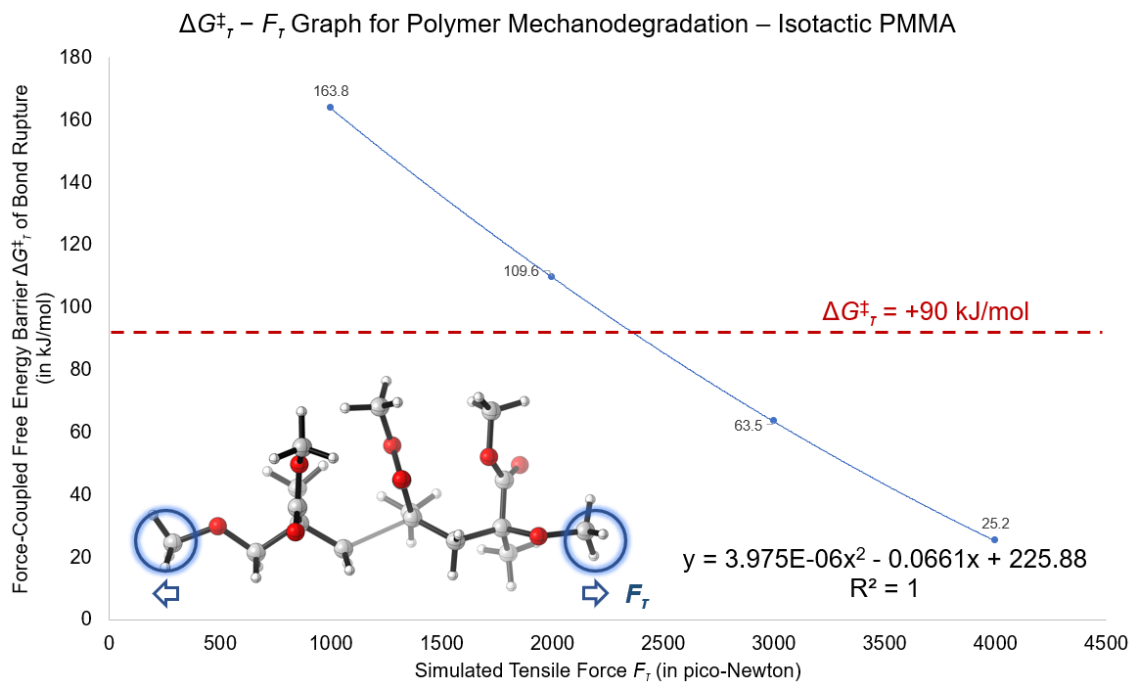
Figure 13. Effect of tensile force F_τ on the force-coupled free energy barrier $\Delta G^{\ddagger}_\tau$ of C-C bond homolysis in isotactic PMMA (please note $\Delta G^{\ddagger}_\tau = 90$ kJ/mol, which corresponds to a $t_{1/2} = 654$ s, is set as the threshold to determine $F_{\text{act}[T, t],\text{calc}}$, considering the timescale of polymer degradation reaction).

Following the same calculation procedure applied on isotactic PMMA, efforts were made to generate the $\Delta G^{\ddagger}_\tau - F_\tau$ equations for all the other polymers (please refer to the SI for the calculation details). Considering the timescale of the mechanodegradation reaction of polymers, the practical force levels $F_{\text{act}[T = 298.15 \text{ K}, t = 654 \text{ s}],\text{calc}}$ (which brings the free energy barrier to the level of $+90$ kJ·mol^{-1}) used to trigger the homolysis in isotactic polymers were summarized in **Table 4**.

Table 4. Computed activation forces $F_{act[T = 298.15\ K,\ t = 654\ s],calc}$ (that bring $\Delta G^{\ddagger}_{\tau}$ to 90 kJ·mol^{-1}) of isotactic polymers (breaking bonds are marked with red color)
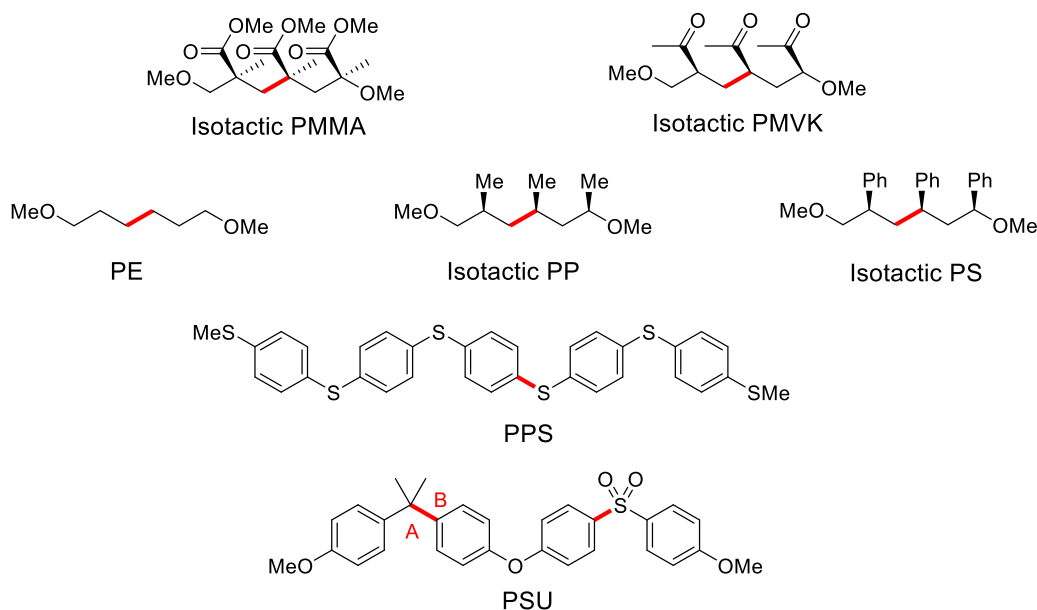
| Polymers	Iso-PMMA	Iso-PMVK	PE	Iso-PP	Iso-PS	PPS	PSU
$F_{act[T = 298.15\ K,\ t = 654\ s],calc}$	2400 pN	2540 pN	3660 pN	3040 pN	2950 pN	1990 pN	1790 pN

It can be easily figured out from **Table 4** that the polymers with C-S bonds embedded are most reactive towards the mechanodegradation. The case of PSU provides a good example of how the C-S bond is sensitive to the external force F_{τ}, since there are two possible cleavage sites, either the C_A-C_B or the C-S(VI) bond. Though this C_A-C_B bond cleavage generates a stable tertiary carbon radical, which is believed to promote such a bond scission, the rupture force of the C-C bond was found as 2760 pN, while that of the C-S bond is only 1790 pN. Even for the C-S bonds, there is a difference in reactivity. The C-S bonds with sulfur in higher oxidation state were found more vulnerable. For example, the C-S(VI) bond in PSU has rupture force $F_{act[T = 298.15\ K,\ t = 654\ s],calc}$ of 1790 pN, which is lower than that of C-S(II) bond in PPS ($F_{act[T = 298.15\ K,\ t = 654\ s],calc}$ = 1990 pN). It is consistent to what Craig and co-workers found experimentally.[31]

It was also found that the C-C bonds in polyethylene (PE) are the most force-resistant among all the polyalkenes. Meanwhile, the polyalkenes possess the highest $F_{act[T = 298.15\ K,\ t = 654\ s],calc}$ if stretched. Compared to PE, introducing the substituent groups to the main chain can reduce $F_{act[T = 298.15\ K,\ t = 654\ s],calc}$, which can be seen from the case of PP and PS. Moreover, the polymers with electron-withdrawing groups (i.e., EWGs) have significantly lower $F_{act[T = 298.15\ K,\ t = 654\ s],calc}$ than their pure polyalkene analogues. For example, the PMMA has a rupture force $F_{act[T = 298.15\ K,\ t = 654\ s],calc}$ of 2400 pN, more than 500 pN lower than that of polystyrene.

Table 5. Computed activation forces $F_{\text{act}[T = 298.15\,K,\ t = 654\,s],\text{calc}}$ (that bring $\Delta G^{\ddagger}_{\tau}$ to 90 kJ·mol^{-1}) of syndiotactic polymers

	Syndiotactic PMMA		Syndiotactic PMMA
	Syndiotactic PP		Syndiotactic PS
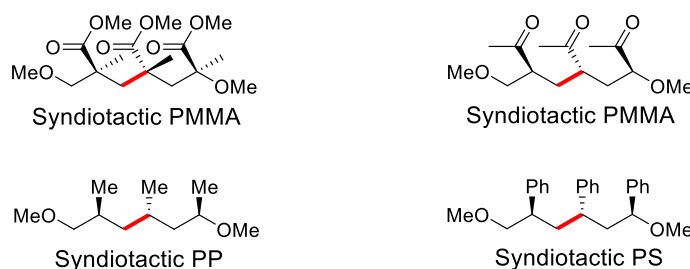
Polymers	Syn-PMMA	Syn-PMVK	Syn-PP	Syn-PS
$F_{\text{act}[T = 298.15\,K,\ t = 654\,s],\text{calc}}$	2430 pN	2880 pN	3410 pN	3180 pN

Calculations of syndiotactic polymers were also conducted (see **Table 5**), and we found that the syndiotactic polymers are more force-resistant if compared to their isotactic isomers. A generally higher $F_{\text{act}[T = 298.15\,K,\ t = 654\,s],\text{calc}}$ was observed for syndiotactic polymers. We noticed that a very recent experimental work from Disendruck and co-workers stated the helical polyglutamates are much more force-responsive than its random coil isomer.[32] The helical polyglutamates are isotactic polymers, and it is consistent to our theoretical study.

To the best of our knowledges, the calculations shown here represent the first detailed computational and quantitative study of how different generic polymers react if treated with external tensile force F_{τ}. It suggests introducing the EWGs to the polyalkenes can greatly facilitate the mechanodegradation. Such a polymer is therefore not a good candidate to hold the reactive mechanophore in the SMFS experiments. Meanwhile, the isotactic polymers are more sensitive to the external force F_{τ}, if compared to its syndiotactic isomer. Polymers with C-S bonds have the potential to be employed as a mechanophore to effectively generate mechanoradicals, as the computed rupture force $F_{\text{act}[T = 298.15\,K,\ t = 654\,s],\text{calc}}$ was found lower than 2000 pN for a force-coupled barrier of 90 kJ·mol^{-1}.

Study on the DN-hydrogel system. The double-network (DN) hydrogels show an extraordinary mechanical property, and can be used as a novel biomedical materials.[33] Recently, Gong and co-workers reported a novel DN-gel system which can undergo a structural reconstruction process to be even more strengthened after a force impact.[34] In such a DN-hydrogel system, a cross-linker molecule helps to connect each PAMPS (i.e., poly(2-acrylamido-2-methyl-1-propanesulfonic acid) polymer chain so that the three-dimensional network structure can be realized. It is envisaged that, once the DN-gel is treated with a stretching force, somewhere near the cross-linker area of the brittle PAMPS network will experience a homolytic bond cleavage. The formed mechanoradicals then interact with monomer existing in the system to trigger a radical polymerization process, thereby reinforcing the material. Therefore, it would be interesting to perform the AFIR calculations on the DN-hydrogel system, from which the results would be helpful to the further design and development of different

DN hydrogel systems. Very recently, a preliminary computational work concerning the force-triggered breaking of covalent bonds in a modeling PAMPS-MBAA (where MBAA stands for *N,N′*-methylenebisacrylamide crosslinker) and a modeling PAMPS-AAC (where AAC stands for azoalkane cross-linker) was reported by us.[19] The calculation results suggested the mechanoradicals can be effectively generated under a relatively small F_τ from PAMPS-AAC network. Compared to the azoalkane cross-linker, there are many possible cleavage sites in the cross-linker of MBAA molecule. Here, instead of using a model molecule composed of two PAMPS chains and one MBAA, we turned our focus on the cross-linker molecule exclusively. Please note that, in our calculations, the double bond of MBAA has been saturated to simulate its status in the polymer network. To systematically study all the possible reactions of MBAA under the external stretching force F_τ, a comprehensive SC-AFIR study, which subsequently generates a reaction path network in a fully automatic manner,[17c,17e] was performed by us.
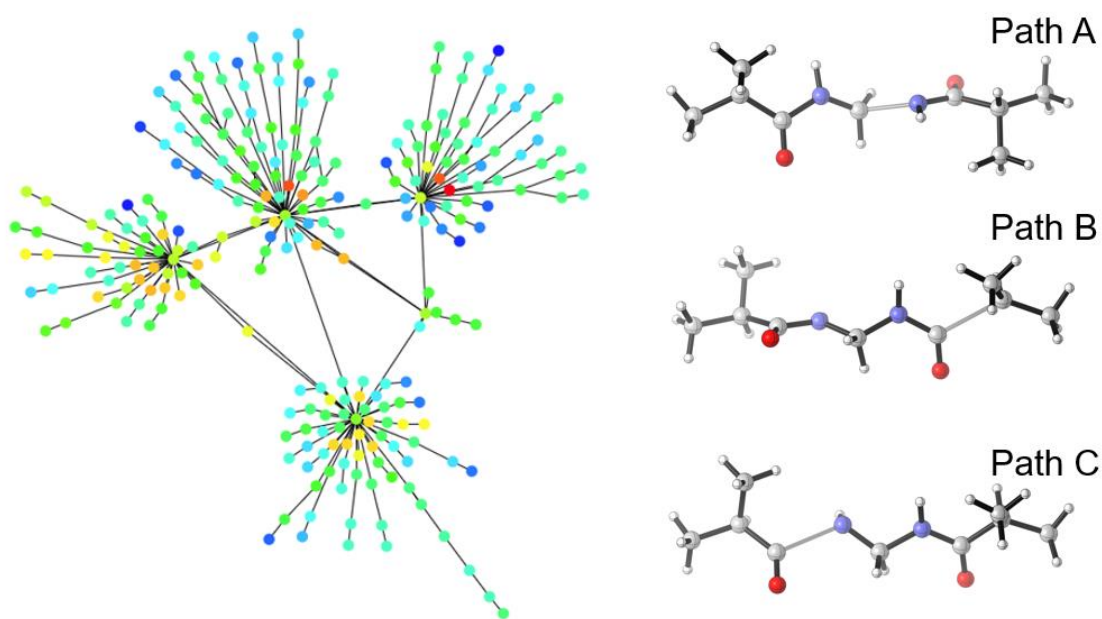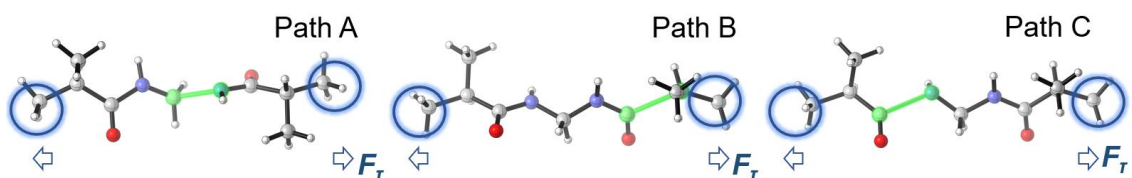

Figure 14. Reaction path network generated by the SC-AFIR calculation (in which each dot represents a minimum structure, and the solid line represents a pathway connecting them) and three main pathways.

Shown in **Figure 14** is the reaction path network generated through our SC-AFIR calculations. A simulated tensile force F_τ of 3000 pN, realized by the AFIR method, is applied to the MBAA molecule (see the highlighted blue part for how the force F_τ is added). A second set of force with α = 7000 pN, which is artificial, was then employed on the entire molecule to trigger reactions under F_τ. In other words, all possible products and their formation pathways were explored systematically by the SC-

AFIR method with τ (in Eq. (3)) = 3000 pN and α (in Eq. (4)) = 7000 pN. Obtained products (i.e., EQs, shown as the dots in **Figure 14**) were further analyzed and categorized into different groups, regarding its bonding connectivity. Based on the grouped EQ structures, in total 37 unique pathways including isomerization and degradation were located for the unimolecular reaction of MBAA under force. Further analysis based on the energy availability indicates that there are in fact three possible mechanodegradation patterns of MBAA and the details is shown in **Figure S24**.

Table 6. Force-coupled free energy barrier $\Delta G^{\ddagger}_{\tau}$ of MBAA degradation under different levels of F_{τ} and the rupture force $F_{\mathrm{act}[T\,=\,298.15\ \mathrm{K},\ t\,=\,654\ \mathrm{s}],\mathrm{calc}}$ (force that brings $\Delta G^{\ddagger}_{\tau}$ to 90 kJ·mol^{-1}) for each degradation pathway (note that the breaking bonds are highlighted in green).

	F_{τ}	Path A (C$_{\mathrm{alkyl}}$-N)	Path B (C$_{\mathrm{acyl}}$-C)	Path C (C$_{\mathrm{acyl}}$-N)
$\Delta G^{\ddagger}_{\tau}$	4000 pN	+46.6 kJ·mol^{-1}	+55.7 kJ·mol^{-1}	+88.1 kJ·mol^{-1}
	3000 pN	+80.6 kJ·mol^{-1}	+105.4 kJ·mol^{-1}	+138.7 kJ·mol^{-1}
	2000 pN	+123.0 kJ·mol^{-1}	+159.9 kJ·mol^{-1}	+198.8 kJ·mol^{-1}
	1000 pN	+182.4 kJ·mol^{-1}	+222.3 kJ·mol^{-1}	+270.6 kJ·mol^{-1}
$F_{\mathrm{act}[T\,=\,298.15\ \mathrm{K},\ t\,=\,654\ \mathrm{s}],\mathrm{calc}}$		2740 pN	3290 pN	3960 pN

The relevant transition states were further studied and re-optimized under force levels ranging from 4000 pN to 1000 pN. Considering the timescale of reaction, which is different from a SMFS test, $\Delta G^{\ddagger}_{\tau}$ = 90 kJ·mol^{-1} was used here to determine $F_{\mathrm{act}[T,\ t],\mathrm{calc}}$, which is labelled as $F_{\mathrm{act}[T\,=\,298.15\ \mathrm{K},\ t\,=\,654\ \mathrm{s}],\mathrm{calc}}$ According to the results, it is found that cleavage of C$_{\mathrm{acyl}}$-N bond (Path C) requires the highest rupture force ($F_{\mathrm{act}[T\,=\,298.15\ \mathrm{K},\ t\,=\,654\ \mathrm{s}],\mathrm{calc}}$ = 3960 pN), which is understandable due to the breaking of -CO-NH- conjugation interaction. The C-C cleavage (Path B), which then generates an acyl radical and a secondary carbon radical, was found having $F_{\mathrm{act}[T\,=\,298.15\ \mathrm{K},\ t\,=\,654\ \mathrm{s}],\mathrm{calc}}$ of 3290 pN. Interestingly, the systematic search of all possible pathways revealed a new degradation pattern, labelled as Path A in **Table 6**. The C$_{\mathrm{alkyl}}$-N bond in the center part of the MBAA molecule can rupture if given F_{τ} = 2740 pN. Indeed, the real DN hydrogel system is much more complex in geometry and the transduction of force within the network is also much more complicated. Many factors will weigh on the possible cleavage sites in the network. Here, the SC-AFIR calculation results showed a vivid image of the systematic search of reaction pathways on the FMPES in an automatic manner. We believe it could be used for the further screening of possible cross-linker molecules used in the multidimensional polymer network.

4. Conclusion

The AFIR method was applied to study the force-assisted ring-opening reaction of a variety of mechanophores and successfully rendered the experimental data obtained through the SMFS experiments. It should be noted that this is the first time we use two sets of forces, of which one explicitly simulates the stretching force that polymer chain feels, and the other, which is artificial, is applied on the covalent bonds of interest to trigger chemical reactions. The former force, named F_τ, helps to construct the FMPES, which allows us to study the mechanochemical reactions on the potential energy surface under the tensile force, including locating the force-coupled transition states. The latter artificial force allows us to explore the force effect on any chemical bonds of interest. In this study, the AFIR method was further employed to study several practical problems encountered in this field. Through the computational study on the retro-Diels-Alder reaction, a special stereo-structural motif, which is believed to enhance the force effect, was revealed. We also evaluated the behaviors of several common polymers under tensile force, and to the best of our knowledge, give the first detailed quantitative report for them. Discussions on the factors that affect the mechanical strength of polymers, for example, the substituent effect and the tacticity effect, was also made in this article. Finally, with the assistance of the AFIR method, a fully automatic search of reaction pathways for a commonly used cross-linker molecule, was realized. Instead of proposing those possible cleavage sites, the AFIR method allows us to systematically study all the possible reactive sites on the FMPES, from which we can work out the rupture force for each bond. Based on the study shown in this article, we believe the AFIR method could be helpful for further study and design of mechanophores and force-responsive polymers.

Computational Details

All of the calculations were performed at the DFT level of theory with the B3LYP hybrid functional[35] as implemented in Gaussian 16.[36] To describe the dispersion properly, an explicit dispersion correction term called GD3,[37] was also employed in the DFT calculations. The 6-311G(d,p) basis set[38] was used for all the atoms (except for Br) involved in this study during both the geometry optimization and the single-point calculation processes. The Stuttgart/Dresden pseudo-potential basis set SDD,[39] as well as a d-polarization function (ζ=0.428),[40] is used for Br atom. To describe the open-shell singlet species involved in the homolysis process, the unrestricted DFT, as well as the procedure to test and optimize the wavefunction were used in this work.[41] To describe the solvation environment in which the molecule stays, the implicit solvation model, IEF-PCM,[42] is applied to all the calculations involved in this study. For the calculations concerning DHC, spiropyran and BCB systems, toluene (ε = 2.3741) was used as the solvent. While in the case of retro-Diels Alder reaction and degradation of MBAA molecule, acetonitrile (ε = 35.688) and water (ε = 78.3553) were employed as the solvents,

respectively. All of the structures were fully optimized with the consideration and constraint of external tensile force. The external tensile force F_τ is properly simulated through our AFIR method. All the geometries shown in this article is visualized by the CYLview software.[43] The calculated activation forces $F_{\text{act}[T, t],\text{calc}}$ are rounded to the nearest tenth.

Associated Content

This material is available free of charge via the Internet at http://pubs.acs.org.

Author Information

Corresponding Author

Julong Jiang - *Department of Chemistry, Faculty of Science, Hokkaido University, Sapporo, 060-8628, Japan;* Email: jjiang.theochem@sci.hokudai.ac.jp

Satoshi Maeda - *Department of Chemistry, Faculty of Science, Hokkaido University, Sapporo, 060-8628, Japan; Institute for Chemical Reaction Design and Discovery (WPI-ICReDD), Hokkaido University, Sapporo 001-0021, Japan;* Email: smaeda@eis.hokudai.ac.jp

Authors

Koji Kubota - *Institute for Chemical Reaction Design and Discovery (WPI-ICReDD), Hokkaido University, Sapporo 001-0021, Japan; Division of Applied Chemistry, Graduate School of Engineering, Hokkaido University, Sapporo, 060-8628, Japan.*

Mingoo Jin - *Institute for Chemical Reaction Design and Discovery (WPI-ICReDD), Hokkaido University, Sapporo 001-0021, Japan; Division of Applied Chemistry, Graduate School of Engineering, Hokkaido University, Sapporo, 060-8628, Japan.*

Zhijian Wang - *Graduate School of Life Science, Hokkaido University, Sapporo, 001-0021, Japan.*

Tasuku Nakajima - *Institute for Chemical Reaction Design and Discovery (WPI-ICReDD), Hokkaido University, Sapporo 001-0021, Japan; Faculty of Advanced Life Science, Hokkaido University, Sapporo 001-0021, Japan.*

Hajime Ito - *Institute for Chemical Reaction Design and Discovery (WPI-ICReDD), Hokkaido University, Sapporo 001-0021, Japan; Division of Applied Chemistry, Graduate School of Engineering, Hokkaido University, Sapporo, 060-8628, Japan.*

Jian Ping Gong - *Institute for Chemical Reaction Design and Discovery (WPI-ICReDD), Hokkaido University, Sapporo 001-0021, Japan; Faculty of Advanced Life Science, Hokkaido University, Sapporo 001-0021, Japan.*

Notes

The authors declare no competing financial interest.

References:

1. (a) Takacs, L. The Historical Development of Mechanochemistry. *Chem. Soc. Rev.* **2013**, *42*, 7649-7659. (b) Do, J. -L.; Friščić, T. Mechanochemistry: A Force of Synthesis. *ACS Cent. Sci.* **2017**, *3*, 13-19. (c)Howard, J. L.; Cao, Q.; Browne, D. L. Mechanochemistry as an Emerging Tool for Molecular Synthesis: What Can it Offer? *Chem. Sci.* **2018**, *9*, 3080-3094. (d) Friščić, T.; Mottillo, C.; Titi, H. M. Mechanochemistry for Synthesis. *Angew. Chem. Int. Ed.* **2020**, *59*, 1018-1029. (e) Willis-Fox, N.; Rognin, E.; Aljohani, T. A.; Daly, R. Polymer Mechanochemistry: Manufacturing Is Now a Force to Be Reckoned with. *Chem* **2018**, *4*, 2499-2537. (f) Hickenboth, C. R.; Moore, J. S.; White, S. R.; Sottos, N. R.; Baudry, J.; Wilson, S. R. Biasing Reaction Pathways with Mechanical Force. *Nature* **2007**, *446*, 423-427. (g) Izak-Nau, E.; Campagna, D.; Baumann, C.; Göstl, R. Polymer Mechanochemistry-Enabled Pericyclic Reactions. *Polym. Chem.* **2020**, *11*, 2274-2299.

2. (a) Subramanian, G.; Mathew, N.; Leiding, J. A Generalized Force-Modified Potential Energy Surface for Mechanochemical Simulations. *J. Chem. Phys.* **2015**, *143*, 134109. (b) Wolinski, K. Exploring Potential Energy Surface with External Forces. *J. Chem. Theory Comput.* **2018**, *14*, 6306-6316. (c) Chen, Z.; Zhu, X.; Yang, J.; Mercer, J. A. M.; Burns, N. Z.; Martínez, T. J.; Xia, Y. The Cascade Unzipping of Ladderane Reveals Dynamic Effects in Mechanochemistry. *Nat. Chem.* **2020**, *12*, 302-309.

3. (a) Sohma, J. Mechanochemistry of Polymers. *Prog. Polym. Sci.* **1989**, *14*, 451-596. (b) Akbulatov, S.; Boulatov, R. Experimental Polymer Mechanochemistry and its Interpretational Frameworks. *ChemPhysChem* **2017**, *18*, 1422-1450. (c) Bowser, B. H.; Craig, S. L. Empowering Mechanochemistry with Multi-mechanophore Polymer Architectures. *Polym. Chem.* **2018**, *9*, 3583-3593. (d) Caruso, M. M.; Davis, D. A.; Shen, Q.; Odom, S. A.; Sottos, N. R.; White, S. R.; Moore, J. S. Mechanically-Induced Chemical Changes in Polymeric Materials. *Chem. Rev.* **2009**, *109*, 5755-5798. (e) Li, J.; Nagamani, C.; Moore, J. S. Polymer Mechanochemistry: From Destructive to Productive. *Acc. Chem. Res.* **2015**, *48*, 2181-2190. (f) Brown, C. L.; Craig, S. L. Molecular Engineering of Mechanophore Activity for Stress-Responsive Polymeric Materials. *Chem. Sci.* **2015**, *6*, 2158-2165. (g) O'Neill, R. T.; Boulatov, R. The Contributions of Model Studies for Fundamental Understanding of Polymer Mechanochemistry. *Synlett* **2022**, *33*, 851-862.

4. (a) Staudinger, H.; Bondy, H. F. Isoprene and Rubber. XIX. The Molecular Size of Rubber and Balata. *Ber. Dtsch. Chem. Ges. B* **1930**, *63*, 734-736. (b) Staudinger, H.; Leupold, E. O. Isoprene and Rubber. XVIII. Studies of the Viscosity of Balata. *Ber. Dtsch. Chem. Ges. B* **1930**, *63*, 730-733. (c) Staudinger, H.; Hener, W. Highly Polymerized Compounds. XCIII. The Breaking Up of the Molecular Fibers of the Polystyrenes. *Ber. Dtsch. Chem. Ges. B* **1934**, *67*, 1159-1164. (d) Odell, J. A.; Keller, A. Flow-Induced Chain Fracture of Isolated Linear Macromolecules in Solution. *J. Polym. Sci. B Polym. Phys.* **1986**, *24*, 1889-1916.

5. (a) Lee, B.; Niu, Z.; Wang, J.; Slebodnick, C.; Craig, S. L. Relative Mechanical Strengths of Weak Bonds in Sonochemical Polymer Mechanochemistry. *J. Am. Chem. Soc.* **2015**, *137*, 10826-10832. (b) Versaw, B. A.; McFadden, M. E.; Husic, C. C.; Robb, M. J. Designing Naphthopyran Mechanophores with Tunable Mechanochromic Behavior. *Chem. Sci.* **2020**, *11*, 4525-4530. (c) McFadden, M. E.; Robb, M. J. Force-Dependent Multicolor Mechanochromism from a Single Mechanophore. *J. Am. Chem. Soc.* **2019**, *141*, 11388-11392. (d) Jung, S.; Yoon, H. J. Heterocyclic Mechanophores in Polymer Mechanochemistry. *Synlett* **2022**, *33*, 863-874. (e) Kumar, S.; Stauch, T. The Activation Efficiency of Mechanophores can be Modulated by Adjacent Polymer Composition. *RSC Adv.* **2021**, *11*, 7391-7396.

6. (a) Lenhardt, J. M.; Black, A. L.; Craig, S. L. Gem-Dichlorocyclopropanes as Abundant and Efficient Mechanophores in Polybutadiene Copolymers under Mechanical Stress. *J. Am. Chem. Soc.* **2009**, *131*, 10818-10819. (b) Black, A. L.; Orlicki, J. A.; Craig, S. L. Mechanochemically Triggered Bond Formation in Solid State Polymers. *J. Mater. Chem.* **2011**, *21*, 8460-8465. (c) Klukovich, H. M.; Kouznetsova, T. B.; Kean, Z. S.; Lenhardt, J. M.; Craig, S. L. A Backbone Lever-arm Effect Enhances Polymer Mechanochemistry. *Nat. Chem.* **2013**, *5*, 110-114. (d) Kean, Z. S.; Black-Ramirez, A. L; Craig, S. L. *J. Polym. Sci. A Polym. Chem.* **2012**, *50*, 3481-3484. (e) Wollenhaupt, M.; Schran, C.; Krupička, M.; Marx, D. Force-Induced Catastrophes on Energy Landscapes: Mechanochemical Manipulation of Downhill and Uphill Bifurcations Explains the Ring-Opening Selectivity of Cyclopropanes. *ChemPhysChem* **2018**, *19*, 837 – 847. (f) Diesendruck, C. E.; Steinberg, B. D.; Sugai, N.; Silberstein, M. N.; Sottos, N. R.; White, S. R.; Braun, P. V.; Moore, J. S. Proton-Coupled Mechanochemical Transduction: A Mechanogenerated Acid. *J. Am. Chem. Soc.* **2012**, *134*, 12446-12449. (g) Kean, Z. S.; Craig, S. L. Mechanochemical Remodeling of Synthetic Polymers. *Polymer* **2012**, *53*, 1035-1048. (h) Wang, J.; Kouznetsova, T. B.; Craig, S. L. Single-Molecule Observation of a Mechanically Activated Cis-to-Trans Cyclopropane Isomerization. *J. Am. Chem. Soc.* **2016**, *138*, 10410-10412. (i) Wang, J.; Kouznetsova, T. B.; Boulatov, R.; Craig, S. L. Mechanical Gating of a Mechanochemical Reaction Cascade. *Nat. Commun.* **2016**, *7*, 13433.

7. (a) Cravotto, G. C.; Cintas, P. Forcing and Controlling Chemical Reactions with Ultrasound. *Angew. Chem. Int. Ed.* **2007**, *46*, 5476-5478. (b) Ribas-Arino, J.; Shiga, M.; Marx, D.

Mechanochemical Transduction of Externally Applied Forces to Mechanophores. *J. Am. Chem. Soc.* **2010**, *132*, 10609–10614. (c) Wang, J.; Piskun, I.; Craig, S. L. Mechanochemical Strengthening of a Multi-mechanophore Benzocyclobutene Polymer. *ACS Macro Lett.* **2015**, *4*, 834-837. (d) Wang, J.; Kouznetsova, T. B.; Niu, Z.; Rheingold, A. L.; Craig, S. L. Accelerating a Mechanically Driven anti-Woodward–Hoffmann Ring Opening with a Polymer Lever Arm Effect. *J. Org. Chem.* **2015**, *80*, 11895-11898. (e) Brown, C. L.; Bowser, B. H.; Meisner, J.; Kouznetsova, T. B.; Seritan, S.; Martinez, T. J.; Craig, S. L. Substituent Effects in Mechanochemical Allowed and Forbidden Cyclobutene Ring-Opening Reactions. *J. Am. Chem. Soc.* **2021**, *143*, 3846-3855.

8. (a) Davis, D. A.; Hamiltion, A.; Yang, J.; Cremar, L. D.; Van Gough, D.; Potisek, S. L.; Ong, M. T.; Braun, P. V.; Martínez, T. J.; White, S. R.; Moore, J. S.; Sottos, N. R. Force-Induced Activation of Covalent Bonds in Mechanoresponsive Polymeric Materials. *Nature* **2009**, *459*, 68-72. (b) Gossweiler, G. R.; Kouznetsova, T. B.; Craig, S, L. Force-Rate Characterization of Two Spiropyran-Based Molecular Force Probes. *J. Am. Chem. Soc.* **2015**, *137*, 6148-6151. (c) Barbee, M. H.; Kouznetsova, T. B.; Barrett, S. L.; Gossweiler, G. R.; Lin, Y.; Rastogi, S. K.; Brittain, W. J.; Craig, S. L. Substituent Effects and Mechanism in a Mechanochemical Reaction. *J. Am. Chem. Soc.* **2018**, *140*, 12746-12750. (d) Kim, T. A.; Robb, M. J.; Moore, J. S.; White, S. R.; Sottos, N. R. Mechanical Reactivity of Two Different Spiropyran Mechanophores in Polydimethylsiloxane. *Macromolecules* **2018**, *51*, 9177-9183. (e) Qiu, W.; Gurr, P. A.; da Silva, G.; Qiao, G. G. Insights into the Mechanochromism of Spiropyran Elastomers. *Polym. Chem.* **2019**, *10*, 1650-1659. (f) Walkey, M. C.; Peiris, C. R.; Ciampi, S.; Aragonès, A. C.; Domínguez-Espíndola, R. B.; Jago, D.; Pulbrook, T.; Skelton, B. W.; Sobolev, A. N.; Díez-Pérez, I.; Piggott, M. J.; Koutsantonis, G. A.; Darwish, N. Chemically and Mechanically Controlled Single-Molecule Switches Using Spiropyrans. *ACS Appl. Mater. Interfaces* **2019**, *11*, 36886–36894. (g) Li, M.; Zhang, Q.; Zhou, Y.; Zhu, S. Let Spiropyran Help Polymers Feel Force. *Prog. Polym. Sci.* **2018**, *79*, 26-39.

9. Blank, K.; Jacobs, M. J. Joining Forces: Integrating the Mechanical and Optical Single Molecule Toolkits. *Chem. Sci.* **2014**, *5*, 1680-1697.

10. (a) Dreuw, A.; Stauch, T. Advances in Quantum Mechanochemistry: Electronic Structure Methods and Force Analysis. *Chem. Rev.* **2016**, *116*, 14137-14180. (b) Akbulatov, S.; Tian, Y.; Boulatov, R. Force–Reactivity Property of a Single Monomer is Sufficient to Predict the Micromechanical Behavior of Its Polymer. *J. Am. Chem. Soc.* **2012**, *134*, 7620–7623. (c) Bettens, T.; Eeckhoudt, J.; Hoffmann, M.; Alonso, M.; Geerlings, P.; Dreuw, A.; De Proft, F. Designing Force Probes Based on Reversible 6π-Electrocyclizations in Polyenes Using Quantum Chemical Calculations. *J. Org. Chem.* **2021**, *86*, 7477–7489. (d) Bettens, T.; Hoffmann, M.; Alonso, M.; Geerlings, P.; Dreuw, A.; De Proft, F. Mechanochemically Triggered Topology Changes in Expanded Porphyrins. *Chem. Eur. J.* **2021**, *27*, 3397–3406.

11. (a) Beyer, M. K. The Mechanical Strength of a Covalent Bond Calculated by Density Functional

Theory. *J. Chem. Phys.* **2000**, *112*, 7307-7312. (b) Klein, I. M.; Husic, C. C.; Kovács, D. P.; Choquette, N. J.; Robb, M. J. Validation of the CoGEF Method as a Predictive Tool for Polymer Mechanochemistry. *J. Am. Chem. Soc.* **2020**, *142*, 16364-16381.

12. (a) Ong, M. T.; Leiding, J.; Tao, H.; Virshup, A. M.; Martínez, T. J. First Principles Dynamics and Minimum Energy Pathways for Mechanochemical Ring Opening of Cyclobutene. *J. Am. Chem. Soc.* **2009**, *131*, 6377-6379. (b) Lenhardt, J. M.; Ong, M. T.; Choe, R.; Evenhuis, C. R.; Martínez, T. J.; Craig, S. L. Trapping a Diradical Transition State by Mechanochemical Polymer Extension. *Science* **2010**, *329*, 1057-1060.

13. (a) Ribas-Arino, J.; Shiga, M.; Marx, D. Understanding Covalent Mechanochemistry. *Angew. Chem. Int. Ed.* **2009**, *48*, 4190-4193. (b) Ribas-Arino, J.; Shiga, M.; Marx, D. Understanding Covalent Mechanochemistry. *Angew. Chem.* **2009**, *121*, 4254-4257.

14. Roessler, A. G.; Zimmerman, P. M. Examining the Ways to Bend and Break Reaction Pathways Using Mechanochemistry. *J. Phys. Chem. B* **2018**, *122*, 6996–7004.

15. (a) Bettens, T.; Alonso, M.; Geerlings, P.; De Proft, F. Implementing the Mechanical Force into the Conceptual DFT Framework: Understanding and Predicting Molecular Mechanochemical Properties. *Phys. Chem. Chem. Phys.* **2019**, *21*, 7378-7388. (b) Bettens, T.; Alonso, M.; Geerlings, P.; De Proft, F. The Hunt for Reactive Alkynes in Bio-orthogonal Click Reactions: Insights from Mechanochemical and Conceptual DFT Calculations. *Chem. Sci.* **2020**, *11*, 1431-1439.

16. (a) Maeda, S.; Ohno, K.; Morokuma, K. Systematic exploration of the mechanism of chemical reactions: the global reaction route mapping (GRRM) strategy using the ADDF and AFIR methods. *Phys. Chem. Chem. Phys.* **2013**, *15*, 3683-3701. (b) Maeda, S.; Harabuchi, Y.; Takagi, M.; Taketsugu, T.; Morokuma, K. Artificial Force Induced Reaction (AFIR) Method for Exploring Quantum Chemical Potential Energy Surfaces. *Chem. Rec.* **2016**, *16*, 2232-2248. (c) Maeda, S.; Harabuchi, Y.; Takagi, M.; Saita, K.; Suzuki, K.; Ichino, T.; Sumiya, T.; Sugiyama, K.; Ono, Y. Implementation and Performance of the Artificial Force Induced Reaction Method in the GRRM17 Program. *J. Comput. Chem.* **2018**, *39*, 233-251. (d) Maeda, S.; Harabuchi, Y. Exploring Paths of Chemical Transformations in Molecular and Periodic Systems: An Approach Utilizing Force. *WIREs Comput. Mol. Sci.* **2021**, *11*, e1538.

17. (a) Sameera, W. M. C.; Maeda, S.; Morokuma, K. Computational Catalysis Using the Artificial Force Induced Reaction Method. *Acc. Chem. Res.* **2016**, *49*, 763-773. (b) Hatanaka, M.; Yoshimura, T.; Maeda, S. Artificial Force Induced Reaction Method for Systematic Elucidation of Mechanism and Selectivity in Organometallic Reactions. *Top. Organomet. Chem.* **2020**, *67*, 57-80. (c) Mita, T.; Harabuchi, Y.; Maeda, S. Discovery of a Synthesis Method for a Difluoroglycine Derivative based on a Path Generated by Quantum Chemical Calculations. *Chem. Sci.* **2020**, *11*, 7569-7577. (d) Sumiya, Y.; Harabuchi, Y.; Nagata, Y.; Maeda, S. Quantum Chemical Calculations to Trace back Reaction Paths for the Prediction of Reactants. *JACS Au* **2022**, *2*, 1181-1188. (e)

Hayashi, H.; Katsuyama, H.; Takano, H.; Harabuchi, Y.; Maeda, S.; Mita, T. In Silico Reaction Screening with Difluorocarbene for N-Difluoroalkylative Dearomatization of Pyridines. *Nat. Synth.* **2022**, *1*, 804-814.

18. (a) Kubota, K.; Toyoshima, N.; Miura, D.; Jiang, J.; Maeda, S.; Jin, M.; Ito, H. Introduction of a Luminophore into Generic Polymers via Mechanoradical Coupling with a Prefluorescent Reagent. *Angew. Chem. Int. Ed.* **2021**, *60*, 16003-16008. (b) Yamamoto, T.; Kato, S.; Aoki, D.; Otsuka, H. A Diarylacetonitrile as a Molecular Probe for the Detection of Polymeric Mechanoradicals in the Bulk State through a Radical Chain-Transfer Mechanism. *Angew. Chem. Int. Ed.* **2021**, *60*, 2680-2683. (c) Peterson, G.; Ko, W.; Hwang, Y. -J.; Choi, T. -L. *Macromolecules* **2020**, *53*, 7795-7802. (d) Yamamoto, T.; Aoki, D.; Otsuka, H. Polystyrene Functionalized with Diarylacetonitrile for the Visualization of Mechanoradicals and Improved Thermal Stability. *ACS Macro Lett.* **2021**, *10*, 744-748. (e) Janke, G.; Schmidt-Naake, G. Synthesis of Block and Graft Copolymers in a Vibratory Mill. *Chem. Eng. Technol.* **2001**, *24*, 711-715. (f) Fukunaga, K.; Kimura, M. Decrease of Molecular Weight of Polystyrene by Ball-milling. *Chem. Lett.* **1987**, *16*, 1503-1506. (g) Sakaguchi, M.; Sohma, J. Copolymerizations Initiated by Mechano-radicals on Particle Surfaces of Poly(tetrafluoroethylene). *J. Appl. Polym. Sci.* **1978**, *22*, 2915-2924. (h) Kondo, S.; Sasai, Y.; Hosaka, S.; Ishikawa, T.; Kuzuya, M. Kinetic Analysis of the Mechanolysis of Polymethylmethacrylate in the Course of Vibratory Ball Milling at Various Mechanical Energy. *J. Polym. Sci. A, Polym. Chem.* **2004**, *42*, 4161-4167. (i) Balema, V. P.; Hlova, I. Z.; Carnahan, S. L.; Seyedi, M.; Dolotko, O.; Rossini, A. J.; Luzinov, I. Depolymerization of Polystyrene under Ambient Conditions. *New J. Chem.* **2021**, *45*, 2935-2938.

19. Wang, Z.; Jiang, J.; Mu, Q.; Maeda, S.; Nakajima, T.; Gong, J. P. Azo-Crosslinked Double-Network Hydrogels Enabling Highly Efficient Mechanoradical Generation. *J. Am. Chem. Soc.* **2022**, *144*, 3154–3161.

20. Choi, C.; Elber, R. Reaction Path Study of Helix Formation in Tetrapeptides: Effect of Side Chains. *J. Chem. Phys.* **1991**, *94*, 751-760.

21. Wang, J.; Kouznetsova, T. B.; Kean, Z. S.; Fan, L.; Mar, B. D.; Martínez, T. J.; Craig, S. L. A Remote Stereochemical Lever Arm Effect in Polymer Mechanochemistry. *J. Am. Chem. Soc.* **2014**, *136*, 15162−15165.

22. (a) Marcus, R. A. Exchange Reactions and Electron Transfer Reactions Including Isotopic Exchange. Theory of Oxidation-Reduction Reactions Involving Electron Transfer. Part 4.—A Statistical-Mechanical Basis for Treating Contributions from Solvent, Ligands, and Inert Salt. *Discuss. Faraday Soc.* **1960**, *29*, 21-31. (b) Marcus, R. A. On the Theory of Oxidation-Reduction Reactions Involving Electron Transfer. V. Comparison and Properties of Electrochemical and Chemical Rate Constants. *J. Phys. Chem.* **1963**, *67*, 853-857. (c) Marcus, R. A. Chemical and Electrochemical Electron-Transfer Theory. *Annu. Rev. Phys. Chem.* **1964**, *15*, 155-196.

23. Wang, J.; Kouznetsova, T. B.; Niu, Z.; Ong, M. T.; Klukovich, H. M.; Rheingold, A. L.; Martinez, T. J.; Craig, S. L. Inducing and Quantifying Forbidden Reactivity with Single-Molecule Polymer Mechanochemistry. *Nat. Chem.* **2015**, *7*, 323-327.

24. Fringuelli, F.; Taticchi, A. Ed., The Diels–Alder Reaction: Selected Practical Methods (Wiley, 2002).

25. (a) Nicolaou, K. C.; Snyder, S. A.; Montagnon, T.; Vassilikogiannakis, G. The Diels–Alder Reaction in Total Synthesis. *Angew. Chem. Int. Ed.* **2002**, *41*, 1668-1698. (b) Briou, B.; Améduri, B.; Boutevin, B. Trends in the Diels–Alder Reaction in Polymer Chemistry. *Chem. Soc. Rev.* **2021**, *50*, 11055-11097. (c) Yang, B.; Gao, S. Recent Advances in the Application of Diels–Alder Reactions Involving o-Quinodimethanes, Aza-o-quinone Methides and O-quinone Methides in Natural Product Total Synthesis. *Chem. Soc. Rev.* **2018**, *47*, 7926-7953. (d) Wessig, P.; Müller, G. The Dehydro-Diels−Alder Reaction. *Chem. Rev.* **2008**, *108*, 2051-2063.

26. (a) Stevenson, R.; De Bo, G. Controlling Reactivity by Geometry in Retro-Diels–Alder Reactions under Tension. *J. Am. Chem. Soc.* **2017**, *139*, 16768-16771. (b) Wu, L. C.; De Bom G. Stereoelectronic Effects in Force-Accelerated Retro-Diels–Alder Reactions. *Synlett* **2022**, *33*, 890-892.

27. (a) Cardosa-Gutierrez, M.; De Bo, G.; Duwez, A. S.; Remacle, F. Steering the Mechanism of the Furan-Maleimide Retro-Diels-Alder Reaction to a Sequential Pathway with an External Mechanical Force. *ChemRxiv* **2022**. (DOI: 10.26434/chemrxiv-2022-g64jp) (b) Cardosa-Gutierrez, M.; De Bo, G.; Duwez, A. -S.; Remacle, F. Bond breaking of Furan-Maleimide Adducts via a Diradical Sequential Mechanism under an External Mechanical Force. *ChemRxiv* **2022**. (DOI: 10.26434/chemrxiv-2022-ccf1x)

28. (a) Lange, J. P. Managing Plastic Waste─Sorting, Recycling, Disposal, and Product Redesign. *ACS Sustainable Chem. Eng.* **2021**, *9*, 15722-15738. (b) Jiang, J.; Shi, K.; Zhang, X.; Yu, K.; Zhang, H.; He, J.; Ju, Y.; Liu, J. From Plastic Waste to Wealth Using Chemical Recycling: A Review. *J. Environ. Chem. Eng.* **2022**, *10*, 106867.

29. Chamas, A.; Moon, H.; Zheng, J.; Qiu, Y.; Tabassum, T.; Jang, J. H.; Abu-Omar, M.; Scott, S. L.; Suh, S. Degradation Rates of Plastics in the Environment. *ACS Sustainable Chem. Eng.* **2020**, *8*, 3494–3511.

30. (a) Kausch, H. -H. Identification of ESR Spectra of Mechanically Formed Free Radicals. In *Polymer Fracture*, 2nd ed.; Kausch, H. -H., Ed.; Springer-Verlag: Berlin, Heidelberg, 1987. (b) Kausch, H. -H. Phenomenology of Free Radical Formation and of Relevant Radical Reactions (Dependence on Strain, Time, and Sample Treatment). In *Polymer Fracture*, 2nd ed.; Kausch, H. -H., Ed.; Springer-Verlag: Berlin, Heidelberg, 1987. (c) Nagamura, T. 14. ESR Study of Polymer Fracture. In *Polymers - Physical Properties*; Fava, R. A., Ed.; Academic Press, 1980. (d) Nagamura, T.; Takayanagi, M. ESR Study of Primary Radical Formation during Mechanical

Degradation of Poly(2,6-dimethyl-p-phenylene oxide) Solid. *J. Polym. Sci., Polym. Phys. Ed.* **1975**, *13*, 567-578.

31. Lin, Y.; Craig, S. L. Oxidative Regulation on the Mechanical Strength of a C-S Bond. *Chem. Sci.* **2020**, *11*, 10444-10448.

32. Zhang, H.; Diesendruck, C. E. Accelerated Mechanochemistry in Helical Polymers. *Angew. Chem. Int. Ed.* **2022**, 61, e202115325.

33. (a) Gong, J. P.; Katsuyama, Y.; Kurokawa, T.; Osada, Y. Double-Network Hydrogels with Extremely High Mechanical Strength. *Adv. Mater.* **2003**, 15, 1155-1158. (b) Haque, M. A.; Kurokawa, T.; Gong, J. P. Super Tough Double Network Hydrogels and Their Application as Biomaterials. *Polymer* **2012**, *53*, 1805-1822. (c) Zhang, H.; Sun, T.; Zhang, A.; Ikura, Y.; Nakajima, T.; Nonoyama, T.; Kurokawa, T.; Ito, O.; Ishitobi, H.; Gong, J. P. Tough Physical Double-Network Hydrogels Based on Amphiphilic Triblock Copolymers. *Adv. Mater.* **2016**, *28*, 4884-4890. (d) Chen, Q.; Chen, H.; Zhu, L.; Zheng, J. Fundamentals of Double Network Hydrogels. *J. Mater. Chem. B* **2015**, *3*, 3654-3676. (e) Fan, H.; Gong, J. P. Fabrication of Bioinspired Hydrogels: Challenges and Opportunities. *Macromolecules* **2020**, *53*, 2769-2782.

34. Matsuda, T.; Kawakami, R.; Namba, R.; Nakajima, T.; Gong, J. P. Mechanoresponsive self-growing hydrogels inspired by muscle training. *Science* **2019**, *363*, 504-508.

35. (a) Becke, A. D. Density-Functional Exchange-Energy Approximation with Correct Asymptotic Behavior. *Phys. Rev. A* **1988**, 38, 3098-3100. (b) Becke, A. D. A New Mixing of Hartree–Fock and Local Density-Functional Theories. J. Chem. Phys. **1993**, *98*, 1372–1377. (c) Lee, C.; Yang, W.; Parr, R. G. Development of the Colle-Salvetti Correlation-Energy Formula into a Functional of the Electron Density. *Phys. Rev. B* **1988**, *37*, 785-789.

36. Gaussian 16, Revision C.01, Frisch, M. J.; Trucks, G. W.; Schlegel, H. B.; Scuseria, G. E.; Robb, M. A.; Cheeseman, J. R.; Scalmani, G.; Barone, V.; Petersson, G. A.; Nakatsuji, H.; Li, X.; Caricato, M.; Marenich, A. V.; Bloino, J.; Janesko, B. G.; Gomperts, R.; Mennucci, B.; Hratchian, H. P.; Ortiz, J. V.; Izmaylov, A. F.; Sonnenberg, J. L.; Williams-Young, D.; Ding, F.; Lipparini, F.; Egidi, F.; Goings, J.; Peng, B.; Petrone, A.; Henderson, T.; Ranasinghe, D.; Zakrzewski, V. G.; Gao, J.; Rega, N.; Zheng, G.; Liang, W.; Hada, M.; Ehara, M.; Toyota, K.; Fukuda, R.; Hasegawa, J.; Ishida, M.; Nakajima, T.; Honda, Y.; Kitao, O.; Nakai, H.; Vreven, T.; Throssell, K.; Montgomery, J. A., Jr.; Peralta, J. E.; Ogliaro, F.; Bearpark, M. J.; Heyd, J. J.; Brothers, E. N.; Kudin, K. N.; Staroverov, V. N.; Keith, T. A.; Kobayashi, R.; Normand, J.; Raghavachari, K.; Rendell, A. P.; Burant, J. C.; Iyengar, S. S.; Tomasi, J.; Cossi, M.; Millam, J. M.; Klene, M.; Adamo, C.; Cammi, R.; Ochterski, J. W.; Martin, R. L.; Morokuma, K.; Farkas, O.; Foresman, J. B.; Fox, D. J. Gaussian, Inc., Wallingford CT, 2016.

37. (a) Grimme, S.; Antony, J.; Ehrlich, S.; Krieg, H. A consistent and accurate ab initio parametrization of density functional dispersion correction (DFT-D) for the 94 elements H-Pu. *J.*

Chem. Phys. **2010**, *132*, 154014. (b) Grimme, S.; Ehrlich, S.; Goerigk, L. Effect of the Damping Function in Dispersion Corrected Density Functional Theory. *J. Comput. Chem.* **2011**, *32*, 1456-1465.

38. (a) McLean, A. D. Contracted Gaussian Basis Sets for Molecular Calculations. I. Second Row Atoms, Z=11–18. *J. Chem. Phys.* **1980**, *72*, 5639-5648. (b) Raghavachari, K.; Binkley, J. S.; Seeger, R.; Pople, J. A. Self-Consistent Molecular Orbital Methods. XX. Basis Set for Correlated Wave Functions. *J. Chem. Phys.* **1980**, *72*, 650-654.

39. (a) Dunning, T. H.; Hay, P. J. "Gaussian Basis Sets for Molecular Calculations" in Methods of Electronic Structure Theory. *Mod. Theor. Chem.* **1976**, *3*, 1-28. (b) Igel-Mann, G.; Stoll, H.; Preuss, H. Pseudopotentials for main group elements (IIIa through VIIa). *Mol. Phys.* **1988**, *65*, 1321-1328.

40. Höllwarth, A.; Böhme, M.; Dapprich, S.; Ehlers, A. W.; Gobbi, A.; Jonas, V.; Köhler, K. F.; Stegmann, R.; Veldkamp, A.; Frenking, G. A Set of d-polarization Functions for Pseudo-Potential Basis Sets of the Main Group Elements Al-Bi and f-type Polarization Functions for Zn, Cd, Hg. *Chem. Phys. Lett.* **1993**, *208*, 237-240.

41. Bauernschmitt, R.; Ahlrichs, R. Stability Analysis for Solutions of the Closed Shell Kohn–Sham Equation. *J. Chem. Phys.* **1996**, *104*, 9047-9052.

42. Scalmani, G.; Frisch, M. J. Continuous Surface Charge Polarizable Continuum Models of Solvation. I. General Formalism. *J. Chem. Phys.* **2010**, *132*, 114110.

43. CYLview, 1.0b; Legault, C. Y. Université de Sherbrooke, 2009.